Review

Review of Research Progress in Nontraditional Machining of Ultrahigh-Temperature Ceramic Matrix Composites

Ya Lu [1,2], Peiyan Sun [3], Xiaohong Yang [4,*], Xudong Guo [2,3], Xiaoke Li [3] and Wuyi Ming [2,*]

1   State Key Laboratory of Digital Manufacturing Equipment and Technology,
    School of Mechanical Science and Engineering, Huazhong University of Science and Technology,
    Wuhan 430074, China
2   Guangdong Provincial Key Laboratory of Manufacturing Equipment Digitization,
    Guangdong HUST Industrial Technology Research Institute, Dongguan 523808, China
3   Henan Key Laboratory of Intelligent Manufacturing of Mechanical Equipment,
    Department of Electromechanical Science and Engineering, Zhengzhou University of Light Industry,
    Zhengzhou 450002, China
4   Hebi Institute of Engineering and Technology, Henan Polytechnic University, Hebi 458030, China
*   Correspondence: yangxiaohong@hpu.edu.cn (X.Y.); mingwuyi@gmail.com (W.M.)

Abstract: Ultrahigh-temperature ceramic matrix composites are currently among the most promising high-temperature-resistant materials, owing to their high-temperature strength, high-toughness and excellent corrosion resistance; they are widely used in national defense and aerospace fields. However, it is a difficult material to machine, and high precision is difficult to achieve using traditional machining methods. Nontraditional machining methods are not constrained by material physical and mechanical properties, and good surface quality is easily obtained, which is an important direction in the field of ultrahigh-temperature ceramic matrix composites. This paper summarizes the recent nontraditional machining methods utilized in the fabrication of ultrahigh-temperature ceramic matrix composites. Firstly, various nontraditional machining methods for ultrahigh-temperature ceramic matrix composites based on borides, carbides and nitrides are reviewed, and the machining performances under different machining conditions are compared. Subsequently, the problems and challenges of ultrahigh-temperature ceramic matrix composite nontraditional machining are summarized and discussed. Lastly, the future development path of nontraditional machining methods for ultrahigh-temperature ceramic matrix composites is summarized and predicted.

Keywords: ultrahigh-temperature ceramic matrix composites; nontraditional machining; electric discharge machining; laser machining; ultrasonic machining

1. Introduction

With the rapid development of science, hypersonic missiles and reusable delivery devices have become important development directions for military aerospace and weapon systems [1]. At present, the main ultrahigh-temperature materials that can be used above 2000 °C are refractory metals, C/C composites and ultrahigh-temperature ceramics. Among these, ultrahigh-temperature ceramic materials are regarded as having the greatest potential in the future ultrahigh-temperature field [2]. Ultrahigh-temperature ceramic materials generally refer to a class of ceramic materials used at high temperatures above 2000 °C, mainly referring to some transition metal borides, carbides and nitrides, such as ZrB_2, HfB_2, TaC, ZrC, HfC and HfN [3]. In addition to having a high melting point of approximately 3000 °C, they also have excellent properties, such as high hardness, high thermal conductivity, good oxidation resistance, good thermal shock resistance and a medium thermal expansion coefficient. Therefore, they are very suitable for use as high-temperature structural materials for supersonic spacecraft, and the application of ultrahigh-temperature ceramic materials in rocket engines has also attracted widespread attention [4,5].

Among them, ultrahigh-temperature ceramic matrix composites (UHTCMCs) are among the most promising high-temperature resistant materials, owing to their advantages of high-temperature strength, good toughness and good corrosion resistance, and they have broad application prospects in the fields of national defense and aerospace [6–8]. Their applications in rocket engine combustion chambers, thrusters, nozzles and hypersonic vehicle thermal protection systems are research hotspots [9,10]. Temperatures higher than 1600 °C, or even 2200 °C, are regarded as the unique requirement of the aerospace industry for ultrahigh-temperatures [11]. Solid rocket engines are typical applications in the ultrahigh-temperature field, where the operating temperature of the nozzle can rise from room temperature to 3000 °C or more in the oxidation environment of high-pressure gases and high-speed particles [12–14]. Therefore, the combustion chamber, propeller and nozzle of a rocket must have a high melting point, superior mechanical qualities and mechanical erosion resistance and oxidation resistance. Hypersonic vehicles are another common application for ultrahigh-temperatures since the thermal protection system of the vehicle must be able to endure extremely high temperatures, high heat flow, vibration and heat load during launch and reentry into space or in the atmosphere [15–17]. The development of thermal protection materials that have strong oxidation resistance, thermal shock resistance, ablation resistance and dimensional stability is required. On the basis of the aforementioned specifications for aerospace ultrahigh-temperature materials, numerous researchers have concentrated on UHTCMCs with excellent high-temperature strength, good fracture toughness, thermal shock resistance, ablation resistance and reliability [18–20].

Low porosity, high strength and good ablative resistance are advantages of UHTCMCs; however, when applied alone, they also have low fracture toughness, poor thermal shock resistance and poor oxidation resistance [21,22]. Due to the brittle nature of the ultrahigh-temperature ceramic composite, it is easy for thermal shock failure to occur during extreme heating, which causes irreparable harm. This has clear limitations for how the material may be used in the context of shock and vibration and is directly tied to the composition and manufacturing method of the ceramic material itself [23]. In order to supplement the damage tolerance and thermal shock resistance of ultrahigh-temperature ceramics, researchers try to use ultrahigh-temperature ceramics as matrices and to adopt various methods to prepare UHTCMCs. UHTCMCs can be employed in a variety of high-temperature situations other than aerospace, including neutron absorbers, fusion first walls, tokamak diverters and fuel rod cladding in the nuclear energy sector [24–26]. They can also be used as a finishing material for plasmas, which include electrodes, cutting tools, refractory materials in metal machining, such as hot well tubes in the refining of steel, and electrical equipment, such as heaters and igniters [20,27,28]. Concentrating solar energy is also one of the most promising renewable energy technologies. In the field of renewable energy, UHTCMCs can be a key component used in receivers to capture and concentrate solar radiation [29]. In the field of aerospace thermal protection, UHTCMCs are the most commonly used ultrahigh-temperature ablation resistant materials. Figure 1 depicts the characteristics and applications of UHTCMCs in the fields of aerospace, national defense, metal smelting, medicine, nuclear energy industry and renewable energy.
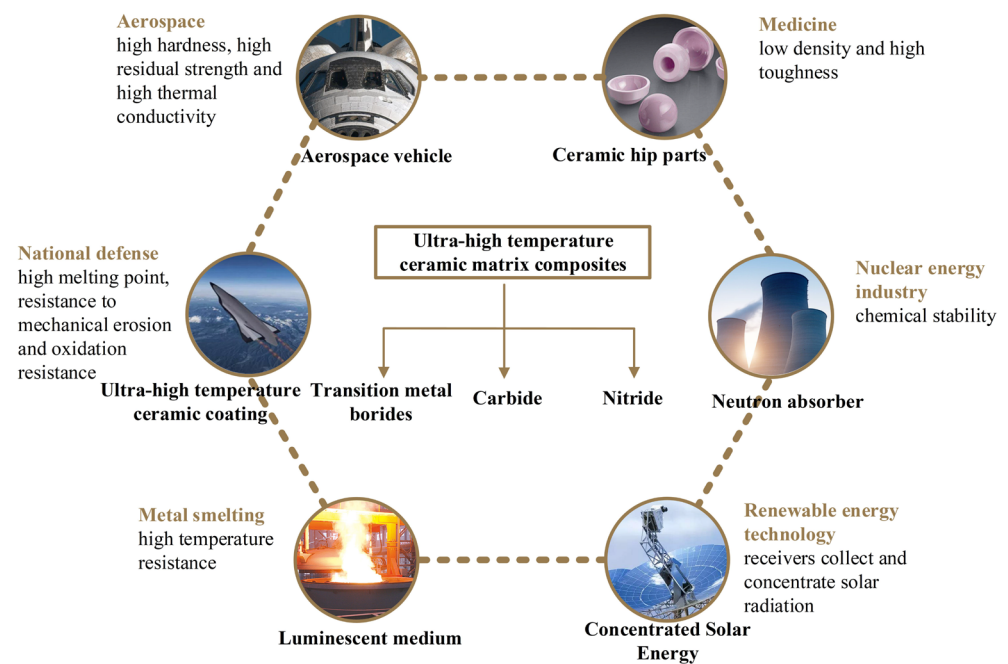
Figure 1. Characteristics and applications of UHTCMCs.

UHTCMCs are typically difficult materials to cut, and it is challenging to machine them with high precision using traditional machining methods [29]. Machining the materials without compromising the characteristics of the ceramics and using machining methods that offer economical solutions while minimizing residual damage represent the main challenges in realizing the full potential of UHTCMCs. The presence of reinforcing particles makes them difficult to machine using conventional machining methods, and the surface roughness and tool wear are too great. As a result, machining costs rise; production times lengthen; and the quality of machined products declines [24]. Considering the main shortcomings of its machinability, the cost of polishing the table accounts for the vast majority of the entire manufacturing cost. Additionally, traditional machining methods can create cracks and stress concentrations on the surface of UHTCMCs, which can weaken the mechanical strength of the part [30]. As a result, a crucial stage in the production of UHTCMC components are identifying affordable and effective machining methods [25]. The majority of conventional machining machines, such as turning, cutting, grinding and drilling, is difficult to use when machining UHTCMCs because they result in significant tool wear, excessive roughness of material surface, low material removal rate, prolonged chatter times and higher costs [31,32]. For example, Satyarthi [33] performed electrical discharge machining (EDM) grinding on ceramic materials. Compared with conventional diamond grinding, the surface finish of nontraditional machining is at least three times that of low-temperature cooled conventional diamond grinding, and the material removal rate is at least four times higher. Machining appears to be impractical for the production of ceramics [26]. Therefore, machining of UHTCMCs can be achieved using a variety of non-traditional methods, including chemical machining [25,27], laser machining [34–37], plasma machining [38–40], electron beam machining [41–43], electrochemical machining [44–48], ultrasonic machining [49–53] and abrasive water jet machining [54–58]. They each have their own advantages and disadvantages. In the production of cutting blades made of cutting ceramics, some surface quality, size and shape parameters are required to provide the function of the blade (machining/cutting certain steels or alloys in a few minutes). In this case, an appropriate technology should be found to provide this quality and appropriate productivity. This review systematically summarizes the research status and development potential of nontraditional machining methods in UHTCMCs. The problems and defects in machining are pointed out. Through the influence of different machining parameters

on the performance of nontraditional machining methods, the machining characteristics and quality of UHTCMCs are analyzed, and the applicability of nontraditional machining methods is analyzed and summarized.

2. Boride-Based UHTCMCs

2.1. Material Properties of Boride-Based UHTCMCs

Ceramic matrix composites based on HfB_2 and ZrB_2 are the most common types of boride-based ceramic matrix composites. By thoughtfully choosing the composition, purity and granularity of the raw materials, the brittleness of the materials can be overcome [59]. They are hard to sinter and densify due to the strength of their covalent connections. This can be resolved by increasing the diffusion rate of the material, delaying the evaporation of the material, accelerating the transmission rate of the material, encouraging the rearrangement of the particles and improving mass transfer kinetics to enhance the sintering performance and increase the density [60]. Due to the formation of the liquid B_2O_3 glass phase, which serves as a good antioxidant defense, single-phase ZrB_2 or HfB_2 exhibits good oxidation resistance below 1200 °C. B_2O_3 rapidly evaporates above 1200 °C, decreasing its usefulness as a diffusion barrier, whereas ZrB_2 or HfB_2 quickly oxidize [61]. When SiC is added, the material's oxidation resistance can be greatly increased. Glassy silicate can also develop on the material's surface at high temperatures, providing good protection below 1600 °C.

In an aspirated hypersonic cruise vehicle design, aerodynamic heating due to viscous dissipation increases with a cubic increase in velocity, which results in a stagnation temperature of about 2400 K at a cruise Mach number of 7. Due to the high L/D ratio, wave rider-derived hypersonic vehicles are used for long cruise missions in which stagnation is experienced along the entire leading edge of the wave rider [62]. Thus, UHTCMCs are frequently key candidates in the hypersonic field for their ability to withstand elevated thermal and pressure loads (i.e., maintain shock under lip conditions) and maintain mechanical properties without changing the aerodynamic shape. In this family of potential materials, composites of ZrB_2 and HfB_2-based ceramics may be the most promising (or most studied) candidates for such applications. This is primarily due to their superior high-temperature properties (mechanical and oxidation) when compared to TiB_2 and TaB_2 [63–65].

2.2. Electrical Discharge Machining of Boride-Based UHTCMCs

By using incredibly hot plasma channels, EDM is able to machine brittle, hard materials with complicated forms without any touch [66,67]. As a result, complicated geometries can be machined using EDM for UHTCMCs [68]. Some researchers have conducted experimental studies on the machining of boride-based UHTCMCs [69–71].

The surface quality analysis of ceramic machining is an important metric for assessing the properties and machining quality of UHTCMCs [72–74]. For the purpose of improving the method and effectiveness of EDM, some studies have looked at the surface quality of boride-based UHTCMCs following EDM. In their study of the EDM performance of ZrB_2–SiC and ZrB_2–SiC–HfB_2 ceramic materials, Monteverde et al. [75] discovered that the surface of these two materials after EDM had Ra of 0.6 μm and 1 μm, respectively, and that micro-cracks and recast materials had appeared on the machined surface. After machining, shell (S), core (C) and leftover glass (G) components were discovered on the surface. Additionally, surface microcracks diminished the material's bending strength by an average of 26.4%. Using microchip-based cylindrical tool electrodes, Li et al. [76] proposed a technique for micro-EDM of ZrB_2–SiC graphite composites. The microporous machining of ZrB_2–SiC graphite composites was more stable with the sheet electrode and had an average machining efficiency that was 3.9 times greater than that of the cylindrical electrode. It was also found that the surface roughness decreased from Ra of 1.56 to 0.97 μm after fine drilling. In their study on the EDM performance of ZrB_2–SiC and NbB_2–SiC

ceramic materials, Malek et al. [77] examined the machining surface and material removal rate (*MRR*) of several materials. The MRR calculation formula is as follows:

$$MRR = \frac{v\left(\mathrm{mm}^3\right)}{t_1\left(\mathrm{min}\right)} = \frac{\pi d^2 h}{4t_1}\left(\mathrm{mm}^3/\mathrm{min}\right)$$

where V is the volume of material removed (unit: mm^3); t_1 is the machining time (unit: min); h is machining depth; and d is the diameter of the tool electrode (unit: mm). Machined workpieces of ZrO_2 and Nb_2O_5 were discovered by X-ray photoelectron spectroscopy (XPS) on the EDM surface, as illustrated in Figure 2a. The results showed that the oxidation of ZrB_2–SiC and NbB_2–SiC occurred in the EDM machine and had a significant effect on the MRR and surface quality. In order to assess the surface roughness of the structure's random region, Han et al. [78] chose a three-dimensional surface roughness measurement system and performed precision electrical machining on complex ZrB_2–SiC structural elements. The results showed that 380 V, 3.5 A, 64 Hz for the pulse shoulder, 64 Hz for the pulse width and 3 mm/min for the maximum line speed were the optimal machining settings. The parameters of Sa, Sz and Sq's surface roughness were 6.3617, 44.4468 and 7.8314 μm, respectively.

The performance of EDM is also influenced by the percentage of reinforcing particles in boride-based UHTCMCs [79,80]. Saha et al. [81] examined the EDM performance of ceramic materials with SiC contents ranging from 5 to 20 wt.% in terms of MRR and surface roughness. They also investigated ZrB_2–SiC ultrahigh-temperature ceramic EDM method. It is discovered that as the SiC concentration increases, so does the volume direct current resistivity of ZrB_2 matrix composites. As SiC increased from 5 wt.% to 20 wt.%, MRR decreased gradually, and resistivity increased steadily from 0.3 cm to 3.5 cm. The main reason was that an increase in SiC concentration reduced the electrical conductivity of ceramic materials, decreasing machining efficiency. The EDM performance of ZrB_2–SiC ceramic matrix composites with various machining parameters for tool materials, such as titanium, tungsten, niobium, graphite and tantalum, was investigated by Sivasankar et al. [82]. The results showed that, when the content of SiC was 20%, the bending strength was higher than other contents. The hardness increased when the SiC content increased, and the MRR of the workpiece increased when the SiC volume percentage increased. With the exception of tantalum, all materials yielded a superior MRR on a workpiece when the SiC percentage was 30 vol.%. Tantalum could produce a higher MRR when the workpiece contained 25% SiC. The 20 vol.% SiC workpiece has a high tool wear ratio (TWR) for all tools. ZrB_2–B_4C composite samples were treated using the EDM procedure by Mandal et al. [83]. The findings indicate that the maximum machining speed and surface roughness occur at a B_4C level of 25 wt.%. For 25 wt.% composite material, the B_4C load showed the maximum hardness (20.49 GPa at 1.0 kgf load). The fracture toughness values of all samples are shown in Figure 2b. Similar to the hardness, the composite showed a higher fracture toughness under a higher B_4C load. ZrB_2–B_4C composite could currently be machined at a maximum speed of 10.56 mm^2/min. ZrB_2–B_4C composites had an average surface roughness Ra of between 1.26 and 5.64 μm. Craters, protrusions and spherical nodules in the sealing layer of the machined surface degraded the surface's quality when the machining speed was increased.
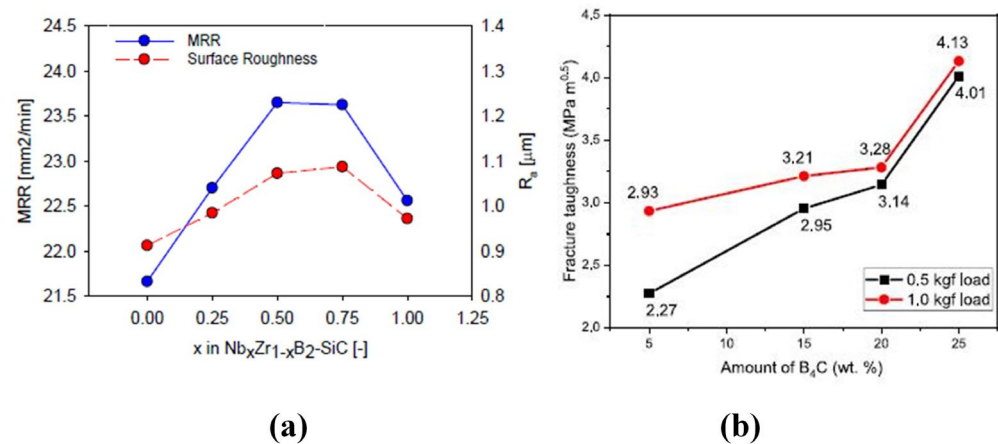
(a)   **(b)**

Figure 2. EDM properties of boride-based UHTCMCs. (**a**) MRR and Surface Roughness Ra for different boride 20 vol.% SiC composite. Reprinted/adapted with permission from Ref. [77]. Copyright 2013, Elsevier. (**b**) Fracture toughness of ZrB_2-B_4C composite with different composition. Reprinted/adapted with permission from Ref. [83]. Copyright 2022, Elsevier.

2.3. Laser Machining of Boride-Based UHTCMCs

Laser machining is also widely used in ceramic machining; this is a wear-free method where the material is not subject to either cutting forces or vibration [32,84–86]. Most notably, compared to conventional and other unconventional technologies, this technique offers a faster cutting speed [87,88]. Numerous researchers have carried out experimental studies to determine whether laser machining of boride-based UHTCMCs is feasible.

Analyzing the surface quality of laser machining boride-based UHTCMCs is a crucial factor in determining how well they machine [36,89]. On the 2024 aluminum alloy matrix, Yang et al. [90] fabricated a ZrO_2 sol-gel composite coating containing laser-ablative SiC whiskers and ZrB_2 particles, as shown in Figure 3a. Under high-intensity continuous laser irradiation, the composite coating exhibits typical pitting morphology with no spalling or breaking. As shown in Figure 3b, when a 6.3 kW/cm^2 laser was used to irradiate the substrate for 10 s, the maximum backside temperature of the substrate was just 150 °C. The oxidation of ZrB_2 and the ZrO_2 layer produced by the ZrO_2 gel can prevent the heat from the laser from transferring through the center ablative crater during laser irradiation. Additionally, the volatilization of B_2O_3 and the cooling effect brought on by SiO_2 and ZrO_2's liquid–solid phase transitions were significant factors in increasing laser ablative resistance. Ideal spiral laser surface treatment was performed by Mahmod et al. [91] on a porous ZrB_2–SiC ceramic composite substrate. The following laser settings were used to create an 8 μm thick uniform glass layer: laser power of 70 W, beam diameter of 1.25 mm, speed of 2 mm/s, acceleration and deceleration rate of 1 mm^2/s. This layer was continuous and prevented further oxidation of the bulk ceramic composite. The structure was well-preserved, and its morphology was similar to that of the initially sintered, non-oxidized pellets. EDS analysis confirms that no oxidation occurred in the internal blocks of ZrB_2–SiC due to the undetectable oxygen element. Wang et al. used three typical materials (ZrB_2, ZrB_2–SiC and ZrB_2–SiC–G (graphite) ceramics) to systematically study the influence of defects on the bending strength of UHTCMCs [92]. The results show that the sensitivity of the material to the flaw angle was in the order ZrB_2–SiC > ZrB_2 > ZrB_2–SiC–G, as shown in Figure 3c. For the same material, a larger defect size led to greater sensitivity of strength to the angle.
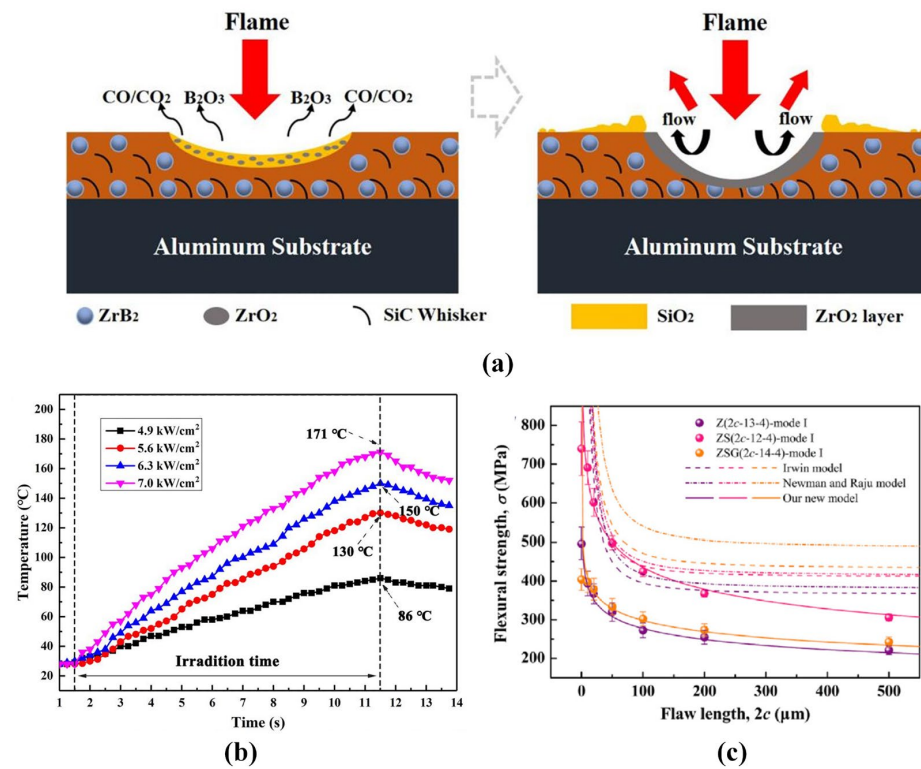
Figure 3. Analysis and schematic diagram of laser machining for boride-based UHTCMCs. (**a**) Laser ablation of composite coating schematic diagram; (**b**) temperature of the back surface substrate at various laser power densities. Reprinted/adapted with permission from Ref. [90]. Copyright 2021, Elsevier. (**c**) Relationship between bending strength and defect length of three ceramics. Reprinted/adapted with permission from Ref. [92]. Copyright 2020, Elsevier.

Lonné et al. [93] irradiated the porous composite ZrB_2 of 39 vol.% SiC with a 90 W low–power moving laser beam under a flowing argon protective atmosphere. According to the findings, the layer thickness approached 20 μm; the temperature reached around 2500 °C; and a SiC–rich fusible phase emerged, partially dissolving ZrB_2 and facilitating its sintering. Also, the surface area achieved almost complete densification. This is because the liquid phase moved toward the sample's surface and bulk after filling the pores. Rudolph et al. [94] investigated how semiconductor SiC and composite SiC–TiC–TiB$_2$ were affected by nanosecond laser pulses in the ultraviolet spectrum and femtosecond laser pulses in the near-infrared spectrum. The findings demonstrated that F_{th} = 0.63 J/cm^2 was the ablation threshold of semiconductor SiC treated by a nanosecond laser pulse in the ultraviolet band. SiC–TiC–TiB$_2$ composite ceramics have an ablation threshold of F_{th} = 1.38 J/cm^2. In contrast, regardless of chemical composition, femtosecond laser pulse machining in the near infrared spectrum yielded a higher value of roughly 1.7 J/cm^2.

2.4. Ultrasonic and Ultrasonic-Assisted Machining of Boride-Based UHTCMCs

Combining the fundamental material removal mechanism of ultrasonic machining with traditional diamond grinding, a greater MRR, increased hole precision and higher surface polish can be achieved at relatively low cost and with minimal environmental impact [95]. Rotary ultrasonic machining (RUM) is a mechanical hybrid machining technique that has the potential to be utilized to treat a wide range of novel and challenging materials, such as boride-based UHTCMCs.

An in-situ combined machining technique using micro-EDM and ultrasonic milling was proposed by Li [96]. In order to improve the machining efficiency and reduce the wear on the electrode length, two tool electrodes of different diameters can be used to

fabricate the micro-nozzles. Large-diameter electrodes are used to remove large amounts of material from the inlet and outlet sections of the micro-nozzle, while small-diameter electrodes are used to manufacture the throat sections. Melting and vaporization were the major mechanisms for material loss, whereas thermal spalling was a secondary factor. The recast layer with a lot of microcracks could be successfully removed, and the surface quality could be improved, by using an ultrasonic amplitude of 2.7 μm as the machining condition for micro-cavity micro-fine ultrasonic milling with particle sizes of 10 μm and a feeding speed of 13 μm/s. Ramulu [97] performed an experimental study on the ultrasonic machining of SiC and 20 vol.% TiB_2/SiC composites. The findings revealed that, in terms of surface roughness, the average Ra value of SiC was typically slightly higher, around 2.0 μm, while the average Ra value of composites was about 1.3 μm. The average Rz value of SiC was also higher, at about 5.4 μm, and the average Rz value of TiB_2/SiC was 4.7 μm.

2.5. Others

In addition to the above nontraditional machining methods, other nontraditional machining methods (such as electron beam melting and plasma machining) are applied to the machining of boride-based UHTCMCs. Electron beam melting (EBM) is an established machine of powder layer-by-layer additive manufacturing metal parts. In their research of the microstructure of produced materials under various machining circumstances, Jia et al. [98] aimed to assess the viability of EBM for the production of boride-based UHTCMCs. Based on the EBM approach, a mathematical model of ZrB_2–30 vol.% $ZrSi_2$ was fabricated, and the machining parameters were then simulated and optimized. The findings indicated that the best machine parameters for the fabrication of ZrB_2–30 vol.% $ZrSi_2$ composites using the EBM technique were 500 W beam power at scanning speeds of 500 mm/s and 1000 W beam power at 1000 mm/s. Pasagada et al. [99] discovered that it was possible to fabricate ZrB_2-based ultrahigh-temperature ceramics components by liquid phase sintering using the EBM method. It has been found that the needle-shaped patterns were produced by melting and solidification change, depending on the input energy density. The impact of the quantity of Ti added on the microstructure growth and phase evolution of ZrB_2–SiC ceramic composites during discharge plasma sintering was investigated by Ghasali et al. [100]. By using high-energy ball milling and spark plasma sintering at 50 MPa pressure for 7 min, ZrB_2–20 vol.% SiC samples with a Ti content of 15 wt.% were fabricated. During the sintering machine, the Ti additive was totally consumed and transformed into the ceramic components TiC, TiB and $TiSi_2$. A further refractory ZrC phase was found as a result of the lateral interaction between ZrB_2 and the SiC and Ti additions. Four components of ZrB_2–SiC–ZrC–C_f UHTCMC were made by Adibpur et al. [101] using a discharge plasma sintering technique. The findings indicated that the greatest characteristics were found in 5% ZrC and 2.5% Cf composites, with a relative density of 99.6%, a hardness of 18 GPa and a bending strength of 565 MPa.

2.6. Summary

In this section, the classification and properties of boride-based UHTCMCs are introduced in detail, and various special machining methods applied to boride-based UHTCMCs are described, including EDM, laser machining, ultrasonic and ultrasonic assisted machining, and other special machining technologies. The machining effects of various methods are described in terms of surface quality, precision, machining cost, etc. applied and obtained. Table 1 depicts the machining effect and application of special machining to boride-based UHTCMCs. However, these technologies cannot simultaneously achieve economical, stable and non-destructive machining of boride-based UHTCMCs. As the preparation of new boride-based UHTCMCs will develop toward homogenization, low porosity and more stable physical and chemical properties [102,103], better nontraditional machining methods need to be developed.

Table 1. Summary of nontraditional machining of boride-based UHTCMCs.

Machining Methods	Materials	Findings	Remarks	Authors, Published Year
EDM	ZrB_2–SiC and ZrB_2–SiC–HfB_2	The Ra of ZrB_2–SiC and ZrB_2–SiC HfB_2 after machining was 0.6 μm and 1 μm, respectively. The Rt measured 4.9 μm and 7.5 μm. The surface microcracks reduce the bending strength by 26.4% on average.	It has been demonstrated to be efficient in the EDM of UHTCMCs sintered parts for more intricate parts.	Monteverde [75], 2008
	ZrB_2–SiC–graphite	The machining efficiency of the sheet electrode was increased by 3.9 times on average; the thin cylindrical electrode could improve the surface quality, and the Ra after finishing was reduced from 1.56 to 0.97 μm.	The use of cylindrical tool electrode can significantly improve the micro EDM.	Li [76], 2017
	ZrB_2–SiC and NbB_2–SiC	When x of (Nb_xZr_{1-x}) B_2–SiC was 0.5 and 0.75, the MRR and Ra of the material were the highest, at 23.7 and 23.6 mm^2/min, and 1.06 and 1.09 μm, respectively.	The presence of transition metal oxides in the heat affected zone has significant influence on the surface quality and removal efficiency of the materials.	Malek [77], 2013
	ZrB_2–SiC	The fracture toughness and bending strength were both 6.5 ± 0.3 Mpa · $m^{1/2}$ and 695.5 ± 13.3 MPa. The surface roughness parameters of Sa, Sz and Sq were 6.3617 μm, 44.4468 μm and 7.8314 μm, respectively.	It can perform precision micro- or mirror–EDM as well as complex structure machining.	Han [78], 2013
	ZrB_2–SiC	The resistivity steadily rose from 0.3 to 3.5 Ω.cm as the SiC concentration grew from 5 to 20%.	It is necessary to clarify the precise ZrB_2–SiC machining mechanism.	Saha [81], 2014
	ZrB_2–SiC	The bending strength and tantalum MRR were highest on the workpiece, with a SiC content of 25% by volume.	The EDM performance of ZrB2–SiC composites is investigated.	Sivasankar [82], 2016
	ZrB_2–B4C	The average Ra was between 1.26 and 5.64 μm when the content of B_4C was 25 wt.%.	The composition with 25 wt.% B4C has the highest machining speed, a dense structure and superior physical and mechanical qualities.	Mandal [83], 2022
Laser machining	ZrO_2 sol–gel composite coating	When the power density was 6.3 kW/cm^2, the maximum back surface temperature of the coating was only 150 °C.	The developed coating can withstand continuous high-energy laser irradiation.	Yang [90], 2021
	ZrB_2–SiC	After surface treatment with 70 W laser on ceramics, about 8.3 ± 1.4 μm thick uniform glass layer.	It offers a substitute for the oxidation machine that occurs in ceramic materials.	Mahmod [91], 2015
	ZrB_2, ZrB_2–SiC and ZrB_2–SiC–G	Using the femtosecond laser method, we successfully manufactured UHTCMCs with controllable size (length of 5–500 μm, depth of 1–51 μm), shape (tip radius of 0.5–6 μm) and direction (angle 0–90°).	Future reliability assessments of brittle structures and the design of high-strength brittle materials will greatly benefit from this.	Wang [92], 2020
	ZrB_2–39 mol.% SiC	Using a 90 W laser, a dense crust with a thickness of more than 20 μm was obtained on a surface area of 0.36 cm^2 in less than 2 min.	This work confirms the feasibility of laser surface densification of porous ZrB_2–SiC pieces.	Lonné [93], 2012
	SiC and SiC–TiC–TiB2	SiC had an ablative threshold of 0.63 J/cm^2, while SiC–TiC–TiB2 composite ceramic had a threshold of 1.38 J/cm^2.	Determined by threshold flows and morphology.	Singh [94], 2003

Table 1. *Cont.*

Machining Methods	Materials	Findings	Remarks	Authors, Published Year
RUM	ZrB_2–SiC–G	The radial and axial machining errors of the 400 μm electrode were less than 16 μm and 17 μm, respectively, and the machining efficiency was 1.6 times higher than that when using a small electrode.	It is possible to realize high-precision combined machining of micro-three-dimensional structures.	Li [96], 2018
	SiC and TiB_2/SiC	The average Ra of TiB_2/SiC composites was 3.7 to 5.90 μm, in which the size of TiB particles was 3 to 5 μm, and the Ra of SiC workpiece materials ranges from 2.1 to 7.54 μm.	The machinability of SiC and TiB_2/SiC was studied systematically.	Ramulu [97], 2005
EBM	ZrB_2–30 vol% $ZrSi_2$	GR had a lower TWR than other tools, especially when the pulse off time was 24 μs, it was less than 1.5 mg/min.	Demonstrated the potential of EBM for additive manufacturing of UHTCMCs with complex geometry.	Jia [98], 2021
	ZrB_2 based UHTC	The machining depth of 700 W sample was 192 ± 20 μm, 165 μm and 139 ± 21 μm.	The EBM system has been validated for use with commercial ultrahigh-temperature superconducting materials.	Pasagada [99], 2022
SPS	ZrB_2–SiC	In the case of ceramic matrix composites, a sintering temperature of 2000 °C and an applied pressure of 50 Mpa were used to result in appropriate densification.	The qualities of sintered ceramic composites may be improved due to ZrB_2's natural fire resistance.	Ghasali [100], 2018
	ZrB_2–SiC–ZrC–C_f	When ZrB_2–18.5 vol.% SiC composites with 5 vol.% ZrC and 2.5 vol.% C_f were enhanced, the material had a relative density of 99.6%, a hardness of 18 GPa and a bending strength of 565 MPa.	Multicomponent composite material sampling method is feasible.	Adibpur [101], 2005

3. Carbide-Based UHTCMCs

3.1. Material Properties of Carbide-Based UHTCMCs

Ceramic matrix composites based on ZrC, HfC, TaC, TiC and other carbides make up the majority of carbide-based UHTCMCs. These compounds have a higher melting point than borides and do not change from a solid phase during heating. They maintain high strength at high temperatures and exhibit good thermal shock resistance [104]. However, this type of carbide ceramic also has very low oxidation resistance and fracture toughness. To overcome the brittleness of ceramics, fiber is usually used to strengthen and toughen them [105,106].

Theoretically, carbide-based UHTCMCs have excellent high temperature resistance, low density, high specific strength and modulus, oxidation resistance, ablative resistance [6,107] and other properties. Carbide-based UHTCMCs have the potential to replace metal as a high-temperature structural material [1]. However, the high-temperature mechanical properties and machining properties conferred on carbide-based UHTCMCs in the current mass production machine are insufficient to meet all of the requirements of aerospace structural parts in extreme environments or long-term use [108,109]. The high-temperature mechanical properties of carbide-based UHTCMCs used in aircraft structural parts are mainly reflected in toughness, high-temperature stability (high-temperature oxidation resistance) and wear resistance. High-toughness is required to withstand high impact, bending and tensile forces during high temperature and high speed operation [110]. High-temperature stability is critical for long-term use in hot environments [104]. In addition, many aircraft structures are subjected to high-speed friction between air and other objects [111]. This requires better wear resistance. Equally important machining properties are related to whether carbide-based UHTCMCs components can achieve the high temperature mechanical properties, mass production and durability required for aircraft [29].

3.2. Electrical Discharge Machining of Carbide-Based UHTCMCs

The study of the relationship between machine parameters and machining performance is an important link to optimize the EDM technology of cemented carbide UHTCMCs [112–114]. Gwon et al. [112] investigated the effect of capacitance and voltage on the conductive SiC–Ti$_2$CN composite during micro-discharge drilling, as well as the inlet clearance, machining time, short circuit number, MRR, count and other variables. According to the experimental findings, SiC–Ti$_2$CN had a higher feed clearance at 2 μm/s than it did at 1 μm/s. The secondary discharge accounted for the increased inlet clearance of SiC–Ti$_2$CN at a feed rate of 2 μm/s. There were essentially no short circuits when the capacitance was 1500 pF or 2000 pF, and the feed rate was 1 μm/s. The EDM performance of Al$_2$O$_3$/SiC$_w$/TiC ceramic composites was explored by Patel et al. [73] and optimized by using the response surface method (RSM). The discharge current was set to 3 A; the pulse width as 10 μs; and the duty cycle as 0.88 to produce the best machining performance. Ra was measured at 1.05 μm under ideal machining conditions, but when discharge current increased, Ra rapidly worsened and then gradually fell after the peaking value. The established model could reliably predict surface roughness within the 95% confidence interval. Al–SiC–B$_4$C composites were cut using the EDM process by Kumar et al. [115] to study the effects of different machining parameters on the slit width and cutting speed during EDM. The statistical significance test was carried out after the mathematical model, and the results were compatible with the findings of the experiment. According to RSM, the ideal machining settings were as follows: 20 A current, 108.6 μs pulse width, 10 mm/min wire feeding speed and 5.65% B$_4$C content. Metal carbide is vulnerable to electrical erosion, and the mechanism of electrical erosion is not yet clear. The challenge for EDM in carbide–based UHTCMCs is to adapt the machine to make electrical corrosion more controllable.

3.3. Laser Machining of Carbide-Based UHTCMCs

The numerical model analysis of laser machining carbide-based UHTCMCs can improve the machining parameters more efficiently [116,117]. Xia [118] studied a nanosecond pulsed laser-induced controlled oxidation-micro-milling coupling method to enhance the micromachining performance of carbide-based UHTCMCs. According to Figure 4a,b, a three-dimensional finite element model was built using the ABAQUS program. The effect of laser machining parameters and auxiliary gases on the oxidation behavior of TiB_2–TiC ceramic composites was investigated, and the effect of laser parameters on temperature field distribution was simulated. The outcomes demonstrated that a strong laser flux would vaporize the oxide and cause the cast layer to develop. When the laser fluence was 10.78 J/cm^2 and the laser scanning speed was 1 mm/s, the irradiated surface had a better oxidation effect, and the subsequent micro-milling machine had a better oxidation effect and a higher MRR. Under the optimal laser parameters, the porous oxide layer was formed, and the thickness of the oxide layer and the oxide layer reached 63 and 22 μm, respectively. In addition, the hardness of the sublayer was much lower than that of the substrate.
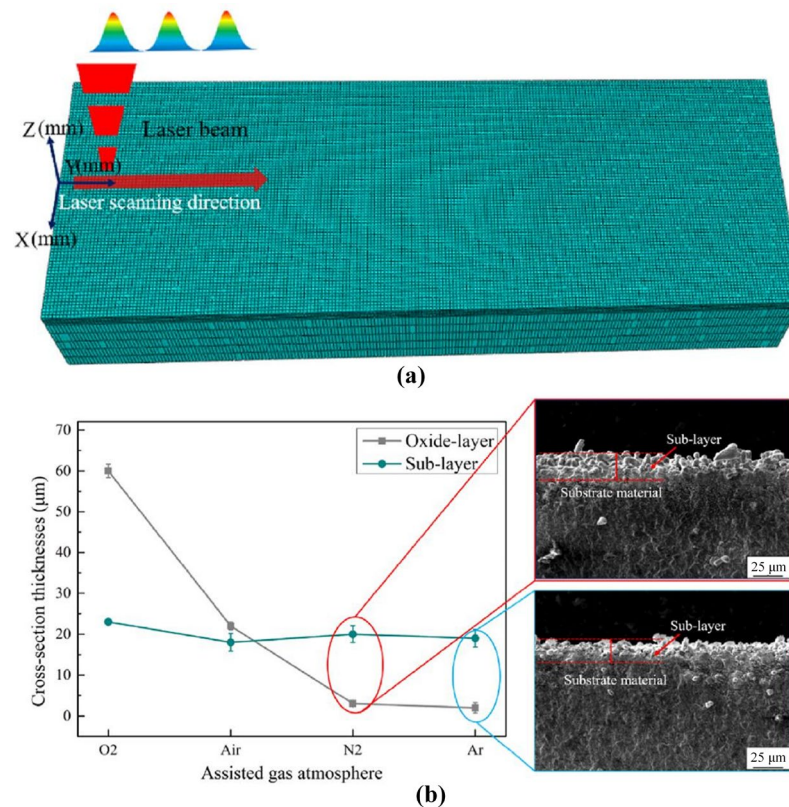

Figure 4. Finite element simulation for laser machining carbide-based UHTCMCs. (**a**) Nanosecond laser-induced controlled oxidation of TiB_2–TiC ceramic composites for subsequent micro-milling; (**b**) sectional thickness of the metamorphic layer in the auxiliary gas environment. Reprinted/adapted with permission from Ref. [118]. Copyright 2022, Elsevier.

Al_2O_3–34 wt.% TiC ceramics, which are increasingly employed in high-precision parts as head sliders, have been machined using laser micromachining by Oliveira et al. [119]. The findings demonstrated a relationship between variations in surface morphology, roughness and clearance rate. Additionally, under laser irradiation, solid solutions of TiC and Al_2O_3 were transformed into TiO_2, $TiC_{0.7}N_{0.3}$ and Al–Ti. On Si_3N_4/TiC ceramic surface by Xing et al. [120], who created two types of regular micro-groove patterns with various geometric properties using a Nd:YAG laser. Friction and wear tests were used to examine the tribological properties of these textured ceramics with and without MoS_2 lubrication. In all experiments, the friction coefficient of the textured ceramics was lower than that

of the smooth ceramics. The wavy grooves among the examined patterns had the best anti-friction effect, and MoS_2 lubrication could extend the wear life of the textured ceramics. By using an oxygen–acetylene torch and high-intensity laser irradiation, Feng et al. [121] assessed the ablative characteristics of ZrC–SiC coatings. The coating had linear and mass ablative rates of –0.37 μm/s and –0.09 mg/s, respectively, and could shield carbon/carbon composites from abrasion for 600 s under oxyacetylene conditions. As shown in Figure 5, the original powder inevitably reacts with oxygen during the spraying machine, and continuous ablation forms a white oxide layer on the entire surface of the sample. However, no obvious defects appear until the ablation time is extended to 600 s, indicating that it has good ablative resistance.

Figure 5. Ablative properties of ZrC–SiC coatings. (**a**) Appearance and (**b**) XRD properties of coatings ablated at various times. Reprinted/adapted with permission from Ref. [121]. Copyright 2022, Elsevier.

3.4. Ion Beam Machining of Carbide-Based UHTCMCs

Ion beam machining (IBM) can efficiently machine carbide-based UHTCMCs [122,123]. With an energy density greater than 10 J/cm^2, Uglov et al. [124] investigated the effects of high-energy pulsed ion beam (HPIB) and compressed plasma flux (CPF) treatment on the phase, element composition, microstructure, hardness and depth of the modified layer of WC–TiC–CO cemented carbide. The findings demonstrate that the fusion of tungsten carbide and titanium carbide particles to generate a tungsten saturated $(W_{1-x}Ti_x)C$ solid solution occurs as the energy density increases in short pulse HPIB. The shock wave produced by the high-power pulse leads to the creation of many cracks in the carbide particles inside and below the melting layer. The melt layer formed through convective mixing of the melt components when the CPF pulse length of 13 to 40 J/cm^2 was prolonged (up to 100 μs) and the thickness of the melt layer was 8 to 10 μm (40 J/cm^2). Two times as hard as untreated cemented carbide, the surface containing a saturated (W1–xTix)C solid solution had a thickness of several microns. Wolfe et al. [125] used ion beam assisted and electron beam physical vapor deposition to fabricate multilayered TiB_2/TiC coatings with varying total layers (2–20) on WC–6 wt.% Co and 0.3 wt.% TaC substrates. As shown in Figure 6a, the results indicated that the average Vickers hardness value increased as the number of layers increased. In addition, the adhesion of the multilayer film with a thickness of 4 μm was higher than 50 N. Wang et al. [126] used an ion beam assisted deposition system to prepare nanoscale TiC/Mo multilayers with a modulated wavelength range from 2.5 to 13.7 nm at a temperature close to ambient. Using nanoindentation method, the multilayer's hardness and elastic modulus were investigated. The findings indicated that the multilayer hardness was greater than the regular mixing value and the maximum hardness, which was almost twice the regular mixing value at 21.40 GPa at = 2.5 nm, as shown in Figure 6b,c. Multilayers also confirmed a dependence on the arrangement of individual layer thicknesses. Multilayers were harder than their hard components after taking individual thickness characteristics (TiC) into account.
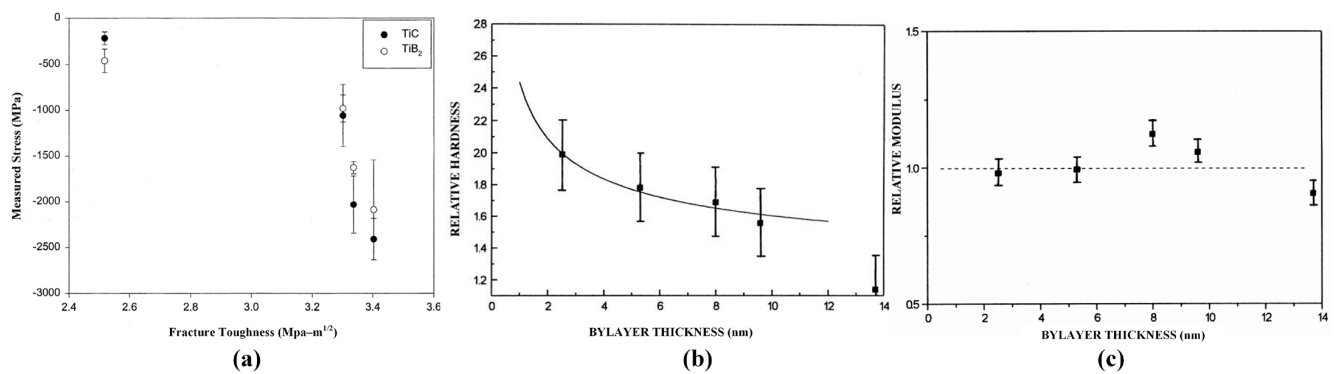
Figure 6. Ion beam machining of carbide-based UHTCMCs. (**a**) Measured stress (MPa) as a function of average fracture toughness (MPa·m$^{1/2}$) for the 14 μm thick TiB$_2$/TiC multilayer coatings deposited on WC–6wt.%Co–0.3wt.%TaC by argon ion beam assisted. Reprinted/adapted with permission from Ref. [125]. Copyright 2003, Elsevier. (**b**) relative hardness and (**c**) elastic modulus of TiC/Mo multilayered films as a function of bilayer thickness. Reprinted/adapted with permission from Ref. [126]. Copyright 2000, Elsevier.

3.5. Others

In addition to the several nontraditional machining methods mentioned above, other nontraditional machining methods (such as electron beam machining and water jet machining) are used to machine carbide-based UHTCMCs. Gao et al. [127] used electron beam melting to fabricate a consistent TiAl matrix structure of dispersed carbides by using a semi-melting stage in the fabrication of TiC/high-Nb–TiAl nanocomposites. Most TiC nanoparticles dissolved during the EBM melting machine, and Ti$_2$AlC was almost spherical, rod-like particles. Carbides had an impact on the TiAl matrix's microstructure deterioration and solidification behavior. Oh et al. [128] investigated the link between the microstructure of (TiC, SiC) yTi–6Al–4V surface composites exposed to high-energy electron beams and their hardness and fracture toughness. On a Ti–6Al–4V substrate, a mixture of TiC, SiC or TiC–SiC powder and CaF$_2$ flux was added. Using an electron beam accelerator, these mixtures were then exposed to an electron beam. Martensite matrix contained a significant number of precipitates (up to 66 vol.%), including TiC and Ti–Si, and formed a surface composite layer that was 1.2–2.1 mm thick. Hard ceramics could be effectively cut and formed using abrasive water jet machining. Al/TiC composites were subjected to abrasive water jet machining by Kiran et al. [129] in order to investigate the impact of various parameters on material removal and surface roughness. The outcomes demonstrated that the MRR and surface roughness were ideal at 2.024 mm^3/min and 2.832 μm, respectively; when the distance was 9 mm, the moving speed was 165 mm/min, and the TiC was 0.9 wt.%.

3.6. Summary

The classification and properties of carbide-based UHTCMCs were described, and various nontraditional machining methods applied to carbide-based UHTCMCs were reviewed, including EDM, laser machining, ion beam machining and other nontraditional machining methods. The machining effect and application of carbide-based UHTCMCs are nontraditional machining shown in Table 2. Because the ceramic matrix of carbide-based UHTCMCs has poor conductivity, the efficiency of electric discharge machining is low. Electrode vibration and deep washing can improve the performance of EDM to a certain extent. The EDM method for machining carbide-based UHTCMCs—such as removal mechanism, molding and machine parameter optimization—still needs to be further studied. The laser machining method can significantly reduce the formation of the oxide layer, and water jet-assisted laser machining can obtain a higher surface quality; however, its cost is high; its precision control is poor; and its machining methods need to be further studied. In addition, it is necessary to further study the machining mechanism by establishing analytical or numerical models [130–132].

Table 2. Summary of nontraditional machining of carbide-based UHTCMCs.

Machining Methods	Materials	Findings	Remarks	Authors, Published Year
EDM	SiC–Ti$_2$CN	The MRR of SiC–Ti$_2$CN and SUS304 converged to about 44,000 μm^3/s and 23,700 μm^3/s, respectively, when the unit discharge energy was high.	Study on micro-EDM properties of novel conductive SiC–Ti$_2$CN composite.	Gwon [112], 2018
	ZrB$_2$–SiC–graphite	Following were the ideal machining parameters: discharged current of 3 A, pulse time of 10 μs and cycle period of 0.88.	This technique is useful for figuring out the best parameter settings for EDM ceramic composites.	Patel [73], 2009
	ZrB$_2$–SiC and NbB$_2$–SiC	The optimum machining conditions were as follows: the current of 20 A, pulse switching time of 108.6 μs, wire feeding speed of 10 mm/min, and B$_4$C content in the composite of 5.65%.	Machinability prediction model	Kumar [115], 2022
Laser machining	TiB$_2$–TiC	Under a laser flux of 10.78 J/cm^2 and a scanning speed of 1 mm/s, the hardness of the sublayer was 9.6 ± 0.7 GPa, which was far lower than the hardness of 20 ± 0.7 GPa.	It offers a theoretical foundation for the upcoming fine milling.	Xia [118], 2022
	Al$_2$O$_3$–34 wt.% TiC	The limit roughness increases from 0.12 to 0.65 mm as the flux increases from 2 to 8 J/cm^2.	Laser micromachining Al$_2$O$_3$–34 wt.%TiC ceramics is proven to be feasible.	Oliveira [119], 1998
	Si$_3$N$_4$/TiC	The friction coefficient was stable at 0.6–0.7 for smooth surfaces and 0.4–0.6 for textured surfaces.	On Si$_3$N$_4$ ceramics, the use of laser surface texturing is discussed.	Xing [120], 2013
	ZrC–SiC	The linear and mass ablation rates of the coating were −0.37 μm/s and −0.09 mg/s, respectively.	Scale evolution of multilayer coatings is discussed in depth.	Feng [121], 2022
IBM	WcTiC–Co	The CPF pulse lasted longer when the energy density was 13~40 J/cm^2.	HPI and CPF are successfully used to improve the mechanical properties and wear resistance of WcTiC–Co.	Uglov [124], 2010
	WC–6wt.%Co	The adhesion of a 4 um multilayer film exceeded 50 nm.	The effect of the total number of TiB coatings on its properties is discussed using various characterization methods.	Wolfe [125], 2003
	TiC/Mo	The highest hardness, 21.40 GPa, was discovered at λ = 2.5 nm.	The possible mechanism of hardening is discussed.	Wang [126], 2000
EBM	TiC/high Nb–TiAl	The microhardness of the material was 433 ± 10HV$_{0.2}$, the ultimate tensile strength was 657 ± 155 MPa and the fracture toughness was 8.1 ± 0.1 MPa√m.	The behavior of solidification and subsequent microstructure degradation are influenced by particles.	Gao [127], 2021
	(TiC, SiC)/Ti–6Al–4V	The thickness of the surface composite layer was basically uniform at 1.2~2.1 mm.	It is expected to serve as the basic data for the selection and application of composite materials.	Oh [128], 2004
AWJM	Al/TiC	The MRR and surface roughness were 2.024 mm^3/min and 2.832 μm, respectively.	Study on water jet machining properties of Al/Tic composites.	Kiran [129], 2020

4. Nitride-Based UHTCMCs

4.1. Material Properties of Nitride-Based UHTCMCs

The matrix of nitride-based UHTCMCs is primarily composed of nitrogen and excess metals (such as titanium, vanadium, niobium, zirconium, tantalum and hafnium), as well as nitride ceramics with aluminum and oxygen in solid solution in silicon nitride while retaining the structure of silicon nitride [133], e.g., ceramics made of silicon nitride, aluminum nitride, boron nitride, etc.

Today, nitride-based UHTCMCs can be seen as a class of materials comparable to steel. Therefore, nitride-based UHTCMCs are prime candidates for a variety of high-temperature applications, such as rotor and stator blades for advanced gas turbines, valves and CAM roller followers for gasoline and diesel engines [134]. On the other hand, the most significant milestone was the use of silicon nitride UHTCMCs as a thermal node component produced by AlliedSignal for aircraft and industrial auxiliary turbine power units, as well as various components used in aircraft turbine engines [135], and as a valve for automotive diesel engines selected by Daimler–Benz. Because of this, producing complex shapes using conventional machining methods is very challenging and expensive, and it can result in cracks on the machined surface [29,136].

4.2. Electrical Discharge Machining of Nitride-Based UHTCMCs

Nitride-based UHTCMCs have been verified to be capable of machining with EDM [137,138]. Using the Taguchi L25 orthogonal test, Selvarajan et al. [139] investigated the EDM characteristics of Si_3N_4–TiN intermetallic compounds and ceramic composites. The machine parameters, including current, pulse opening and closing times, spark gap voltage and dielectric pressure, were optimized by taking into account the measured response. Gray correlation analysis was used to calculate the ideal performance characteristics. The measurements were as follows: spark gap voltage = 40 V; dielectric pressure = 18 kg/cm^2; current = 7 A; pulse off time = 9 μs; and pulse on time = 7 μs. ATZ ($ZrO_2Al_2O_3$) and Si_3N_4–TiN are two different ceramic composites whose ablative behavior was examined by Schubert et al. [140]. Experiments were conducted to evaluate the highest aspect ratio of the micro-hole that could be produced, the surface quality that resulted and the viability of machining intricate 3D structures by EDM. The findings demonstrated that in order to get a high MRR, a certain set of parameters must be established because the material properties of ceramic composites are strongly dependent on their mixing ratio. As a result, the ideal parameter range for oxide ceramics, such as ATZ, was found to be between 40 and 60 μJ, whereas for non–oxide ceramics, such as Si_3N_4–TiN, the ideal parameter range was between 100 and 110 μJ, as shown in Figure 7. Si_3N_4–TiN exhibits unique ablative behavior, with an MRR of 200% compared to ATZ, as a result of the breakdown of Si_3N_4–TiN at high temperatures in the discharge zone. In their investigation of the impact of micro-EDM milling performance on Si_3N_4–TiN workpieces, Marrocco et al. [141] examined MRR and TWR in relation to discharge pulse types to assess how various pulse forms affected the performance indices of such micro-EDM. Analysis revealed that MRR was solely responsive to normal pulses for the set of machine parameters taken into account, with other pulse types having no discernible impact. However, the presence of arcing and delayed pulses resulted in an unanticipated improvement in tool wear, whereas the TWR was adversely affected by regular pulses. The surface of the Si_3N_4–TiN micro-EDM was examined using SEM and EDS, and it was discovered that there were resolidified droplets and microcracks, which altered the chemical composition and surface quality of the ensuing micro-machining features. Bucciotti et al. [142] investigated and assessed the EDM machining method while researching the microstructure, mechanical characteristics and toxicological characteristics of Si_3N_4–TiN ceramic composites. Si_3N_4–TiN's mechanical and microstructural characteristics demonstrated that it had the potential to function as a biomaterial that could replace load-bearing prostheses. The development of Si_3N_4–TiN as a biomaterial and the use of EDM to create devices with a near-net shape were thus encouraged.
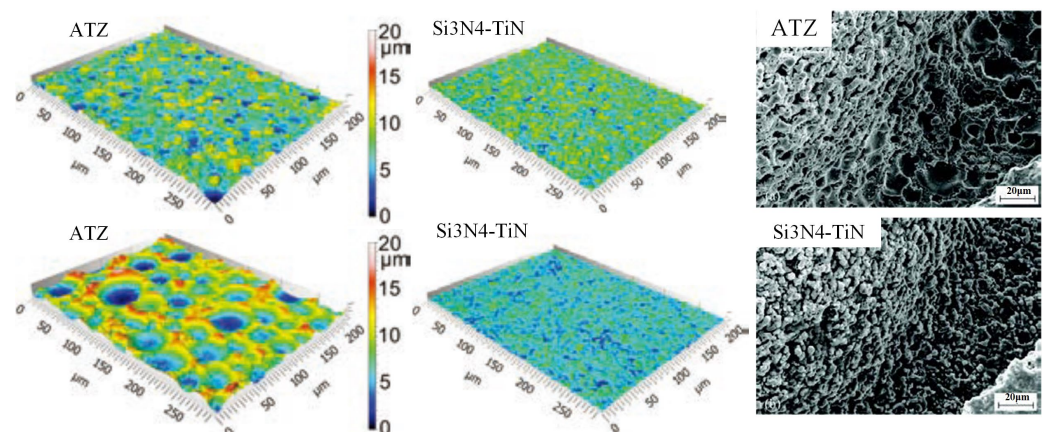

Figure 7. Surface quality analysis and electron microscopy of ATZ and Si_3N_4–TiN before and after machining. Reprinted/adapted with permission from Ref. [140]. Copyright 2016, Elsevier.

4.3. Laser Machining of Nitride-Based UHTCMCs

In recent years, lasers have been widely used in nitride-based UHTCMCs machining [143–146]. TiN/Si_3N_4 was machined using a Nd:YAG laser by Campbell and Islam [147], who also examined the rate of material removal, the surface roughness and the likelihood of microcracks. The findings demonstrated that TiN/Si_3N_4 had a MRR as high as 110 mm^3/min. The surface roughness was impacted by the pulse energy. The lower the energy, the smoother the surface. In the range between 0.8 and 1.0 J/pulse, the average surface roughness was 0.81 μm. The effectiveness of material removal was unaffected by plasma production, even when the overlapped pulse frequency was as high as 75%. On ceramic composites made of Si_3N_4 and TiC, Vlasova et al. [148] performed laser ablation research. The findings demonstrated that Si_3N_4/TiC would break down when exposed to laser light, and these compounds would also split into Si, Ti and N_2. The byproducts of laser-induced ablation was deposited as composite glass (amorphous) sheets after being oxidized to SiO_2 and TiO_2 as they traveled through the atmosphere containing $O_2 + N_2$. $TiSi_2$, which participated in the ablation machine and absorbed Ti, Al and Y atoms/oxides in the film, was partially formed by the Y_2O_3 and Al_2O_3 impurities in the laser ablation ceramics. In order to create a sequence of linear parallel micro-grooves on the surface of the samples, Tshabalala et al. [144] treated Si_3N_4–SiC composite samples using a nanosecond Nd:YAG laser system under various laser energy (0.1~0.6 mJ) and lateral pulse overlap (50%~88%). The findings demonstrated that when pulse energy and transverse overlap increased, material removal increased logarithmically. The ideal surface texture was attained at a combination of 0.3 mJ (2.38×105 J/m^2) and 50% pulse energy, and transverse pulse overlap, as illustrated in Figure 8. The material removal threshold was set at 0.1 mJ (0.78×105 J/m^2).
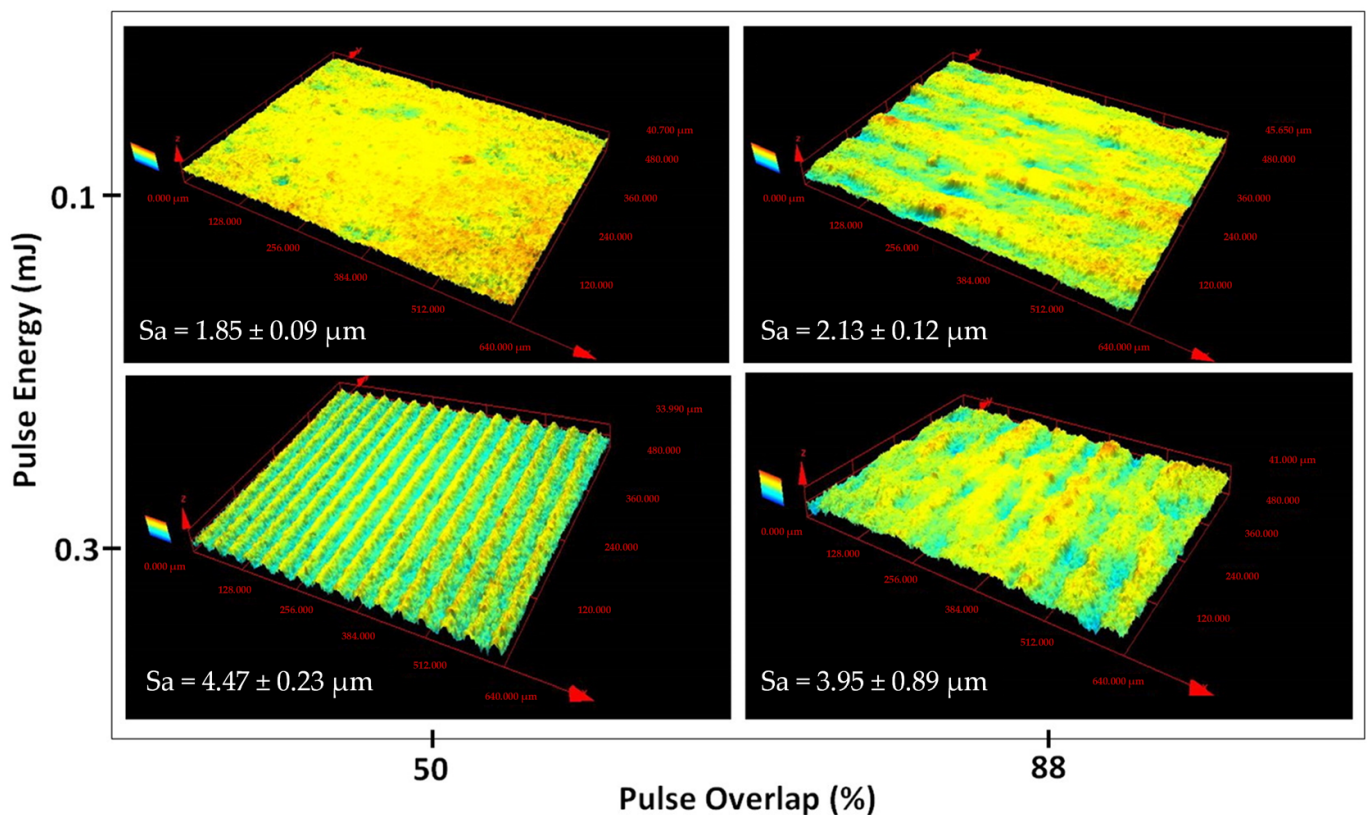

Figure 8. Three–dimensional surface topography image by confocal laser scanning microscope. Reprinted/adapted with permission from Ref. [144]. Copyright 2016, Elsevier.

In order to create a high-quality microchannel bionic texture on a Si_3N_4/TiC ceramic surface, Xing et al. [149] investigated the effects of nanosecond laser machine parameters with a wavelength of 1064 nm on the surface quality and geometry of microchannels. The findings demonstrated that the laser machine settings had a significant impact on the microchannel's surface morphology and geometry. Larger channel depth and width were often produced by increased laser power, slower scanning speeds, higher frequencies and higher sweep frequencies due to more energy accumulation. For microchannel machining, laser machine parameters of 10 W of power, 20 kHz of frequency and 50 mm/s of scanning speed were ideal. Xing et al. [150] used a femtosecond pulsed laser with a pulse width of 120 fs, a wavelength of 800 nm and a repetition frequency of 1000 Hz to create several parallel nanoscale grooves on the surface of Si_3N_4/TiC ceramics. The ideal values were 2.5 μJ pulse energy, 130 μm/s of speed and a single-pass. Increases in pulse energy and decreases in scanning speed result in deeper grooves. Surface roughness rose as pulse energy, scanning speed and scanning times increased.

4.4. Ion Beam Machining of Nitride-Based UHTCMCs

Using a dual ion beam technique, Colligon et al. [151] produced hard nanocomposite TiN/Si_3N_4 coatings on Si. An analysis of the coating's cross-section, using high-resolution transmission electron microscopy, revealed that the ion–assisted microstructure transforms from an unaided columnar structure to the presence of tiny crystals in the amorphous seepage network. When ion-assisted energy was increased for Si substrates that were not heated, microhardness values rose from 24 to 29 GPa, whereas for substrates that were deposited at 400 °C, microhardness values were 7 to 8 GPa or higher. The coatings' microhardness values remained unchanged even after annealing at 1000 °C, demonstrating their remarkable thermal stability. Direct ion lithography and a Ga-focused ion beam were utilized by Mitrofanov et al. [152] to illustrate the feasibility of creating a submicron window in the Si_3N_4/GaN shield. The Si_3N_4 mask after Ga-focused ion beam etching had good quality and no imperfections according to a substrate surface analysis. SEM pictures showing the creation of fringed surfaces provided further evidence of the selective growth materials' high crystal quality.

4.5. Summary

In this section, nitride-based UHTCMCs are introduced in terms of composition, properties and limitations of traditional machining. A variety of nontraditional machining methods for nitride-based UHTCMCs, including EDM, laser machining and ion beam machining, are summarized. The optimization of electrical parameters in EDM can improve the machining quality, and the optimization of laser machine parameters can obtain the best surface texture of nitride-based UHTCMCs microchannels. The machining effects and applications of nontraditional machining of nitride-based UHTCMCs are shown in Table 3. In comparison to boride- and carbide-based UHTCMCs, relatively little research has been conducted on nontraditional machining of nitride-based UHTCMCs.

Table 3. Machining performance of nitride-based UHTCMCs.

Machining Methods	Materials	Findings	Remarks	Authors, Published Year
EDM	Si_3N_4–TiN	The best performance parameters resulted in a current of 7 A, a pulse opening time of 7 μs, a pulse closing time of 9 μs, a dielectric pressure of 18 kg/cm^2 and a spark gap voltage of 40 V.	This method can effectively improve the spark corrosion machine.	Selvarajan [139], 2016
	ATZ and Si_3N_4–TiN	The range of the optimization parameter set was found to be between 40 and 60 μJ for ATZ and between 100 and 110 μJ for Si_3N_4–TiN.	It encouraged using Si_3N_4–TiN in biomedicine.	Schuber [140], 2016
	Si_3N_4–TiN	The surface roughness Ra measured after micro-EDM was between 0.77 and 0.98 μm, and the initial roughness Ra of the workpiece was between 0.16 and 0.30 μm.	Evaluation of the effect of discharge pulse shape on micro-EDM performance	Marrocco [141], 2020
	Si_3N_4–TiN	The Ra value of the material was 1.40 ± 0.15 μm on the flat surface and the machined surface.	Encourages further research on Si_3N_4–TiN as a biomaterial.	Bucciotti [142], 2010
Laser machining	TiN/Si_3N_4	Between 0.8 and 1.0 J/pulse, the surface roughness was 0.81 μm on average.	Verifying the feasibility of laser machining TiN/Si_3N_4.	Campbell [147], 1995
	Si_3N_4/TiC	The SiO_2 halo was first formed during the ablation machine at E ≈ 5 J. At E ≈ 10 J, a halo that could be attributed to Ti appeared.	To open up new opportunities for modifying surface characteristics and producing nanomaterials for a number of technical fields.	Vlasova [148], 2020
	Si_3N_4–SiC	Material removal threshold was set at 0.1 mJ (0.78×105 J/m^2).	Exploring the material response during PLM surface texturing.	Tshabalala [144], 2016
	Si_3N_4/TiC	The optimized laser machining parameters were as follows: laser power of 10 W, frequency of 20 kHz, scanning speed of 50 mm/s and one overscan.	The effect of laser parameters on microchannels is studied.	Xing [149], 2021
	Si_3N_4/TiC	The ideal parameters were a 2.5 μJ pulse energy, a scan speed of 130 μm/s and a single-pass scan.	The use of a femtosecond pulsed laser in the surface nanobraiding of ceramics based on Si_3N_4 is very important.	Xing [150], 2014
IBM	TiN/Si_3N_4	The microhardness values for the substrate that was deposited at 400 °C were 7–8 GPa or higher.	These coatings are highly thermally stable.	Colligon [151], 2005
	Si_3N_4/GaN	After FIB etching, the etching depth of the material was 6–7 nm, and the average Ra was 0.53 nm.	The obtained results can be used for the prototyping of submicron photonic and electronic structures.	Mitrofanov [152], 2017

5. Discussions

UHTCMCs are widely used in aerospace, automobiles, manufacturing and other fields due to their high wear resistance, corrosion resistance and low density. However, the performance of UHTCMCs can be negatively impacted by material surface and subsurface degradation, such as microcracks, during machining. Ceramic engineering enhances the method for machining materials but degrades their mechanical qualities. Traditional machining of UHTCMCs has drawbacks such as significant tool wear and inevitable machining flaws. Most research focuses on the removal mechanism of UHTCMCs, parameter optimization and tool selection. To reduce machining defects, the traditional machining methods for UHTCMCs need to be further optimized. This includes developing new tool structures and optimizing machine parameters. Table 4 shows a relative comparison of different machining methods [30].

Table 4. Relative comparison between different nontraditional methods. Reprinted/adapted with permission from Ref. [30]. Copyright 2020, Elsevier.

Machining Machine	Parameter Influencing Economy					
	Capital Investment	Toolings/ Fixtures	Power Requirements	Removal Efficiency	Roughness of Surface	Tool Wear Ratio
Electrical discharge machining	Medium	High	Low	High	Medium	High
Laser machining	Medium	Low	Very low	Very high	Medium	Very low
Ultrasonic machining	Low	Low	Low	High	Very Low	Medium
Electrochemical machining	Very high	Medium	Medium	Low	Low	Very low
Plasma arc machining	Very low	Low	Very low	Very low	Very high	Very low
Chemical machining	Medium	Low	High	Medium	Low	Very low
Conventional machining	Low	Low	Low	Very low	Very Low	Low

(1) Figure 9 compares the machining efficiency, machining accuracy, machining cost and environmental impact of different nontraditional machining methods of UHTCMCs. Compared with other machining methods, the EDM machine is a green machining method with less pollution and a low cost. It has the potential to prepare surfaces with excellent antifouling properties [153]. EDM is frequently used to machine UHTCMCs because it is not constrained by the workpiece's hardness, tensile strength, toughness or other mechanical qualities [154]. At the same time, the EDM of UHTCMCs has a high material removal rate. For example, Si_3N_4–TiN exhibits a unique ablation behavior during EDM, and the MRR is 200% compared with ATZ [140]. However, selecting an auxiliary electrode that is appropriate for a specific industrial application for a variety of UHTC–EDM machining is complicated and difficult because many different factors must be considered, such as the properties of the ceramic material, the size and formation of acoustic emissions, the machining performance indices and many others. This requires extensive numerical and experimental studies on establishing a machine database of different UHTCMCs [155].
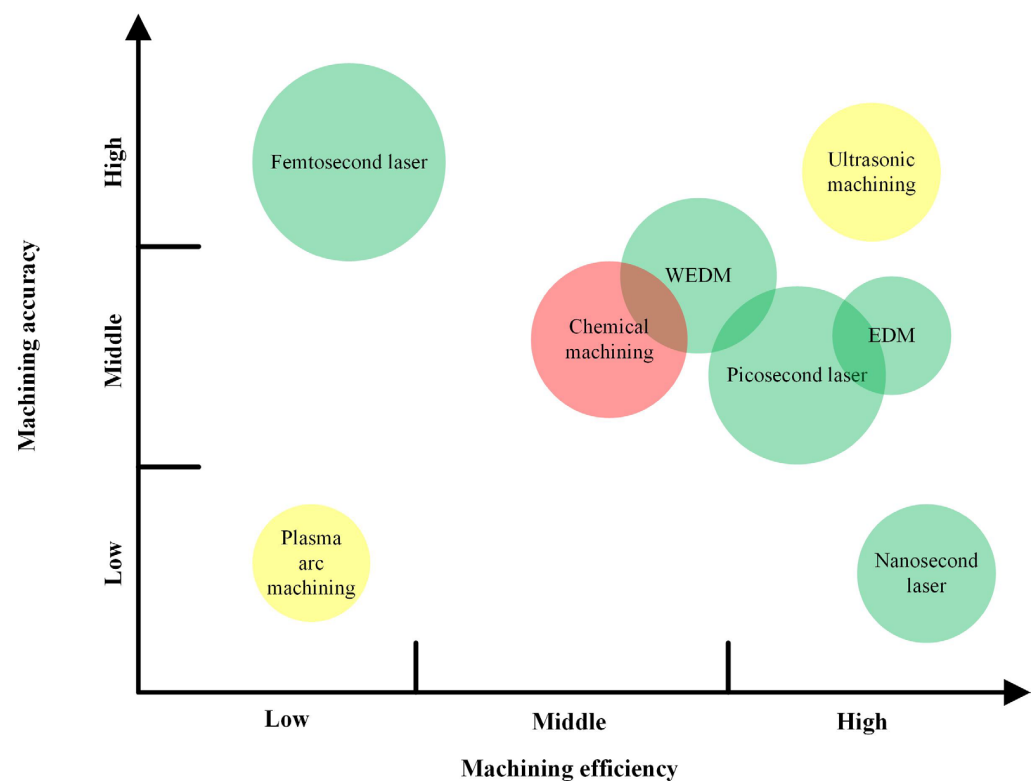

Figure 9. Machining efficiency, precision, cost and environmental impact of different nontraditional machining methods of UHTCMCs. (The radius of the circle indicates the machining cost; the larger the radius, the higher the cost. The color of the circle indicates the environmental impact of manufacturing, while green, yellow and red indicate small, medium and large impacts).

(2) Although laser machining does not have the problems of tool wear, delamination and burr defects during machining and has high machining efficiency, there are heat-affected zones and ablated oxide layers on the surface of UHTCMCs after machining. The area of the heat-affected zone and the thickness of the ablated oxide layer can be decreased using the ultrashort pulse (such as femtosecond laser) method, optimized laser settings and the addition of protective gas. For example, Mahmod [91] performed laser machining on UHTCMCs after optimizing laser settings with a femtosecond laser. A better laser surface treatment was achieved, and the thickness of the ablative oxide layer was reduced to 8.3 μm, about 60% of that before optimization. The laser machining method of UHTCMCs still needs to be based on numerical simulation software. The removal mechanism of ultrahigh-temperature ceramic matrix composites was thoroughly

investigated using laser ablation experiments, and new technological measures were proposed to reduce the area of the heat-affected zone and the thickness of the ablation oxide layer.

(3) In comparison to traditional machining, ultrasonic vibration-assisted machining minimizes tool wear and, to a certain extent, suppresses delamination and burr flaws. At the same time, ultrasonic machining has a better machining effect on UHTCMCs. The Ra of TiB_2/SiC is about 35% lower than that of SiC, and the Rz is about 13% lower than that of SiC [97]. Although ultrasonic vibration-assisted machining increases the precision of the machining, machining flaws cannot be entirely avoided, and the price of a complete set of ultrasonic vibration–assisted machining equipment makes it impractical to use on a large scale in actual production. At the same time, in order to improve the machining quality of UHTCMCs, it is also necessary to further investigate the coupling mechanism between the ultrasonic vibration tool and the material, the mechanism via which the material is removed when vibrated, the development of new ultrasonic vibration equipment, the optimization of the machine, etc.

(4) Lastly, although research on machining UHTCMCs using other nontraditional machining methods (ion beam, electron beam, water jet, etc.) or hybrid machining methods has been carried out; overall, the machining methods need to be improved. The influence of different machine parameters and types of different UHTCMCs should be considered in the experimental machining, and the possibility of efficient, precise, stable and non-destructive machining should also be explored.

6. Conclusions

This review summarized the current state of research and development potential for nontraditional machining methods in the machining of UHTCMCs, in addition to highlighting machining problems and defects. Some prospects that can be considered for nontraditional machining of UHTCMCs are described below:

1. Nontraditional machining methods need a series of technical innovations to meet the requirements of UHTCMCs machining. In addition, it is necessary to establish an analytical or numerical model to understand the cutting mechanics, in addition to further preliminary studies in the basic areas of the removal mechanism of UHTCMCs.
2. The study of how various UHTCMCs material removal processes affect their mechanical properties (i.e., fatigue, creep and degradation) is of great interest to the aerospace and nuclear sectors.
3. The development of machining methods suitable for UHTCMCs is still in its early stages. For example, some researchers use diamond abrasive cutting technology to machine UHTCMCs, but the machining time is long and the tool wear is too large, increasing the machining cost by 60%–90% [156]. Researchers in the machining field need to work with materials scientists to explore more efficient and reliable methods of machining UHTCMCs.
4. Due to the specificity of nontraditional machining, some machining techniques have a negative impact on the environment. In the future, the large-scale machining and manufacturing of UHTCMCs should not only consider the machining efficiency and machining cost but should also consider the impact on the environment.

Author Contributions: Conceptualization, Y.L., X.Y. and W.M.; methodology, P.S. and X.Y.; formal analysis, P.S. and X.G.; investigation, X.Y. and X.L.; resources, Y.L. and W.M.; writing—original draft preparation, Y.L. and P.S.; writing—review and editing, X.Y. and W.M.; visualization, P.S. and X.G.; supervision, X.Y. and W.M. All authors have read and agreed to the published version of the manuscript.

Institutional Review Board Statement: Not applicable.

Informed Consent Statement: Not applicable.

Data Availability Statement: Not applicable.

Conflicts of Interest: The authors declare no conflict of interest.

References

1. Padture, N.P. Advanced structural ceramics in aerospace propulsion. *Nat. Mater.* **2016**, *15*, 804–809. [CrossRef] [PubMed]
2. Johnson, S.; Gasch, M.; Stackpoole, M.; Lawson, J.; Gusman, M. Recent developments in ultra high temperature ceramics at NASA ames. In Proceedings of the 16th AIAA/DLR/DGLR International Space Planes and Hypersonic Systems and Technologies Conference, Bremen, Germany, 19–22 October 2009; p. 7219.
3. Fahrenholtz, W.G.; Hilmas, G.E. Ultra-high temperature ceramics: Materials for extreme environments. *Scr. Mater.* **2017**, *129*, 94–99. [CrossRef]
4. Xie, W.; Peng, Z.; Jin, H.; Meng, S.; Pan, Y. Fabrication and thermal structural characteristics of ultra-high temperature ceramic struts in scramjets. *J. Wuhan Univ. Technol. Mater. Sci. Ed.* **2018**, *33*, 375–380. [CrossRef]
5. Grashchenkov, D.V.; Sorokin, O.Y.; Lebedeva, Y.E.; Vaganova, M.L. Specific features of sintering of HfB2-based refractory ceramic by hybrid spark plasma sintering. *Russ. J. Appl. Chem.* **2015**, *88*, 386–393. [CrossRef]
6. Wang, X.; Gao, X.; Zhang, Z.; Cheng, L.; Ma, H.; Yang, W. Advances in modifications and high-temperature applications of silicon carbide ceramic matrix composites in aerospace: A focused review. *J. Eur. Ceram. Soc.* **2021**, *41*, 4671–4688. [CrossRef]
7. Kodama, H.; Sakamoto, H.; Miyoshi, T. Silicon Carbide Monofilament-Reinforced Silicon Nitride or Silicon Carbide Matrix Composites. *J. Am. Ceram. Soc.* **1989**, *72*, 551–558. [CrossRef]
8. Misra, A.K. Thermochemical Analysis of the Silicon Carbide-Alumina Reaction with Reference to Liquid-Phase Sintering of Silicon Carbide. *J. Am. Ceram. Soc.* **1991**, *74*, 345–351. [CrossRef]
9. Li, Q.; Dong, S.; Wang, Z.; Shi, G. Fabrication and properties of 3-D Cf/ZrB2–ZrC–SiC composites via polymer infiltration and pyrolysis. *Ceram. Int.* **2013**, *39*, 5937–5941. [CrossRef]
10. Gao, Y.; Zha, B.-L.; Wang, J.-J.; Sun, Z.-S.; Zhang, Z.-F.; Shi, Y.-A. Ablation mechanism of C/C–SiC and C/C–SiC–ZrC composites in hypersonic oxygen-enriched environment. *Ceram. Int.* **2022**, *48*, 22985–22993. [CrossRef]
11. Sayir, A. Carbon fiber reinforced hafnium carbide composite. *J. Mater. Sci.* **2004**, *39*, 5995–6003. [CrossRef]
12. Bianchi, D.; Nasuti, F.; Martelli, E. Coupled analysis of flow and surface ablation in carbon-carbon rocket nozzles. *J. Spacecr. Rocket.* **2009**, *46*, 492–500. [CrossRef]
13. Bianchi, D.; Nasuti, F.; Onofri, M.; Martelli, E. Thermochemical erosion analysis for chraphite/carbon-carbon rocket nozzles. *J. Propuls. Power* **2011**, *27*, 197–205. [CrossRef]
14. Thakre, P.; Yang, V. Chemical erosion of carbon-carbon/graphite nozzles in solid-propellant rocket motors. *J. Propuls. Power* **2008**, *24*, 822–833. [CrossRef]
15. Squire, T.H.; Marschall, J. Material property requirements for analysis and design of UHTC components in hypersonic applications. *J. Eur. Ceram. Soc.* **2010**, *30*, 2239–2251. [CrossRef]
16. Hu, P.; Guolin, W.; Wang, Z. Oxidation mechanism and resistance of ZrB2–SiC composites. *Corros. Sci.* **2009**, *51*, 2724–2732. [CrossRef]
17. Liu, W.-H.; Luo, Z.-S. Research advances of aerodynamic heating for hypersonic aircraft. *Aero Weapon.* **2014**, *6*, 8–13.
18. Glass, D. Ceramic matrix composite (CMC) thermal protection systems (TPS) and hot structures for hypersonic vehicles. In Proceedings of the 15th AIAA international space planes and hypersonic systems and technologies conference, Dayton, OH, USA, 28 April–1 May 2008; p. 2682.
19. Huang, J.-F.; Zeng, X.-R.; Li, H.-J.; Xiong, X.-B.; Sun, G. ZrO2–SiO2 gradient multilayer oxidation protective coating for SiC coated carbon/carbon composites. *Surf. Coat. Technol.* **2005**, *190*, 255–259. [CrossRef]
20. Yan, B.; Chen, Z.; Zhu, J.; Zhang, J.; Jiang, Y. Effects of ablation at different regions in three-dimensional orthogonal C/SiC composites ablated by oxyacetylene torch at 1800 °C. *J. Mater. Process. Technol.* **2009**, *209*, 3438–3443. [CrossRef]
21. Chevykalova, L.A.; Kelina, I.Y.; Mikhal'chik, I.L.; Arakcheev, A.V.; Plyasunkova, L.A.; Kasimovskii, A.A.; Matyushin, K.S. Preparation of ultra-high temperature ceramic material based on zirconium boride by SPS method. *Refract. Ind. Ceram.* **2014**, *54*, 455–462. [CrossRef]
22. Hillig, W.B. Prospects for ultra-high-temperature ceramic composites. In *Tailoring Multiphase and Composite Ceramics*; Springer: New York, NY, USA, 1986; pp. 697–712.
23. Gasch, M.J.; Ellerby, D.T.; Johnson, S.M. Ultra high temperature ceramic composites. In *Handbook of Ceramic Composites*; Springer: New York, NY, USA, 2005; pp. 197–224.
24. Kumar, M.; Singh, H. Multi response optimization in wire electrical discharge machining of Inconel X-750 using Taguchi's technique and grey relational analysis. *Cogent Eng.* **2016**, *3*, 1266123. [CrossRef]
25. Rozenek, M.; Kozak, J.; Dąbrowski, L.; Lubkowski, K. Electrical discharge machining characteristics of metal matrix composites. *J. Mater. Process. Technol.* **2001**, *109*, 367–370. [CrossRef]

26. Tuersley, I.P.; Jawaid, A.; Pashby, I.R. Various methods of machining advanced ceramic materials. *J. Mater. Process. Technol.* **1994**, *42*, 377–390. [CrossRef]

27. Yao, Y.X.; Wang, B.; Wang, J.H.; Jin, H.L.; Zhang, Y.F.; Dong, S. Chemical machining of Zerodur material with atmospheric pressure plasma jet. *CIRP Ann.* **2010**, *59*, 337–340. [CrossRef]

28. Shimpi, J.R.; Sidhaye, D.S.; Prasad, B.L. Digestive ripening: A fine chemical machining process on the nanoscale. *Langmuir* **2017**, *33*, 9491–9507. [CrossRef] [PubMed]

29. Binner, J.; Porter, M.; Baker, B.; Zou, J.; Venkatachalam, V.; Diaz, V.R.; D'Angio, A.; Ramanujam, P.; Zhang, T.; Murthy, T. Selection, processing, properties and applications of ultra-high temperature ceramic matrix composites, UHTCMCs—A review. *Int. Mater. Rev.* **2020**, *65*, 389–444. [CrossRef]

30. Ming, W.; Jia, H.; Zhang, H.; Zhang, Z.; Liu, K.; Du, J.; Shen, F.; Zhang, G. A comprehensive review of electric discharge machining of advanced ceramics. *Ceram. Int.* **2020**, *46*, 21813–21838. [CrossRef]

31. Volosova, M.A.; Stebulyanin, M.M.; Gurin, V.D.; Melnik, Y.A. Influence of Surface Layer Condition of Al_2O_3+TiC Ceramic Inserts on Quality of Deposited Coatings and Reliability during Hardened Steel Milling. *Coatings* **2022**, *12*, 1801. [CrossRef]

32. Ming, W.; Guo, X.; Xu, Y.; Zhang, G.; Jiang, Z.; Li, Y.; Li, X. Progress in non-traditional machining of amorphous alloys. *Ceram. Int.* **2023**, *49*, 1585–1604. [CrossRef]

33. Satyarthi, M.K.; Pandey, P.M. Comparison of EDG, diamond grinding, and EDM processing of conductive alumina ceramic composite. *Mater. Manuf. Process.* **2013**, *28*, 369–374. [CrossRef]

34. Romoli, L.; Tantussi, G.; Dini, G. Experimental approach to the laser machining of PMMA substrates for the fabrication of microfluidic devices. *Opt. Lasers Eng.* **2011**, *49*, 419–427. [CrossRef]

35. Li, Z.L.; Zheng, H.Y.; Lim, G.C.; Chu, P.L.; Li, L. Study on UV laser machining quality of carbon fibre reinforced composites. *Compos. Part A Appl. Sci. Manuf.* **2010**, *41*, 1403–1408. [CrossRef]

36. Samant, A.N.; Dahotre, N.B. Laser machining of structural ceramics—A review. *J. Eur. Ceram. Soc.* **2009**, *29*, 969–993. [CrossRef]

37. Pham, D.T.; Dimov, S.S.; Ji, C.; Petkov, P.V.; Dobrev, T. Laser milling as a 'rapid' micromanufacturing process. *Proc. Inst. Mech. Eng. Part B J. Eng. Manuf.* **2004**, *218*, 1–7. [CrossRef]

38. Shi, B.; Dai, Y.; Xie, X.; Li, S.; Zhou, L. Arc-enhanced plasma machining technology for high efficiency machining of silicon carbide. *Plasma Chem. Plasma Process.* **2016**, *36*, 891–900. [CrossRef]

39. Malhotra, R.; Saxena, I.; Ehmann, K.; Cao, J. Laser-induced plasma micro-machining (LIPMM) for enhanced productivity and flexibility in laser-based micro-machining processes. *CIRP Ann.* **2013**, *62*, 211–214. [CrossRef]

40. Junge, P.; Greinacher, M.; Kober, D.; Stargardt, P.; Rupprecht, C. Metastable Phase Formation, Microstructure, and Dielectric Properties in Plasma-Sprayed Alumina Ceramic Coatings. *Coatings* **2022**, *12*, 1847. [CrossRef]

41. Spinney, P.S.; Howitt, D.G.; Smith, R.L.; Collins, S.D. Nanopore formation by low-energy focused electron beam machining. *Nanotechnology* **2010**, *21*, 375301. [CrossRef]

42. Parthasarathy, J.; Starly, B.; Raman, S.; Christensen, A. Mechanical evaluation of porous titanium (Ti6Al4V) structures with electron beam melting (EBM). *J. Mech. Behav. Biomed. Mater.* **2010**, *3*, 249–259. [CrossRef]

43. Koike, M.; Martinez, K.; Guo, L.; Chahine, G.; Kovacevic, R.; Okabe, T. Evaluation of titanium alloy fabricated using electron beam melting system for dental applications. *J. Mater. Process. Technol.* **2011**, *211*, 1400–1408. [CrossRef]

44. Rajurkar, K.P.; Sundaram, M.M.; Malshe, A.P. Review of electrochemical and electrodischarge machining. *Procedia CIRP* **2013**, *6*, 13–26. [CrossRef]

45. Acharya, B.R.; Mohanty, C.P.; Mahapatra, S.S. Multi-objective optimization of electrochemical machining of hardened steel using NSGAII. *Procedia Eng.* **2013**, *51*, 554–560. [CrossRef]

46. Holstein, N.; Krauss, W.; Konys, J. Development of novel tungsten processing technologies for electro-chemical machining (ECM) of plasma facing components. *Fusion Eng. Des.* **2011**, *86*, 1611–1615. [CrossRef]

47. Chen, S.-T.; Jiang, Z.-H.; Wu, Y.-Y.; Yang, H.-Y. Development of a grinding–drilling technique for holing optical grade glass. *Int. J. Mach. Tools Manuf.* **2011**, *51*, 95–103. [CrossRef]

48. Zhao, R.; Huang, L.; Zhao, H.; Cao, Y.; Tian, W.; Wang, N. Study of Mask Electrochemical Machining for Ring Narrow Groove under the Action of Multiple Physical Fields. *Coatings* **2022**, *12*, 605. [CrossRef]

49. Ning, F.D.; Cong, W.L.; Pei, Z.J.; Treadwell, C. Rotary ultrasonic machining of CFRP: A comparison with grinding. *Ultrasonics* **2016**, *66*, 125–132. [CrossRef]

50. Rao, R.V.; Pawar, P.J.; Davim, J.P. Parameter optimization of ultrasonic machining process using nontraditional optimization algorithms. *Mater. Manuf. Process.* **2010**, *25*, 1120–1130. [CrossRef]

51. Liu, D.; Cong, W.L.; Pei, Z.J.; Tang, Y. A cutting force model for rotary ultrasonic machining of brittle materials. *Int. J. Mach. Tools Manuf.* **2012**, *52*, 77–84. [CrossRef]

52. Singh, R.P.; Singhal, S. An experimental study on rotary ultrasonic machining of macor ceramic. *Proc. Inst. Mech. Eng. Part B J. Eng. Manuf.* **2018**, *232*, 1221–1234. [CrossRef]

53. Singh, R.P.; Singhal, S. Experimental investigation of machining characteristics in rotary ultrasonic machining of quartz ceramic. *Proc. Inst. Mech. Eng. Part L J. Mater. Des. Appl.* **2018**, *232*, 870–889. [CrossRef]

54. Alberdi, A.; Rivero, A.; López de Lacalle, L.N.; Etxeberria, I.; Suárez, A. Effect of process parameter on the kerf geometry in abrasive water jet milling. *Int. J. Adv. Manuf. Technol.* **2010**, *51*, 467–480. [CrossRef]

55. Ting, H.T.; Abou-El-Hossein, K.A.; Chua, H.B. Review of micromachining of ceramics by etching. *Trans. Nonferrous Met. Soc. China* **2009**, *19*, s1–s16. [CrossRef]

56. Matsumura, T.; Muramatsu, T.; Fueki, S. Abrasive water jet machining of glass with stagnation effect. *CIRP Ann.* **2011**, *60*, 355–358. [CrossRef]

57. Gupta, V.; Pandey, P.M.; Garg, M.P.; Khanna, R.; Batra, N.K. Minimization of kerf taper angle and kerf width using Taguchi's method in abrasive water jet machining of marble. *Procedia Mater. Sci.* **2014**, *6*, 140–149. [CrossRef]

58. Deris, A.M.; Zain, A.M.; Sallehuddin, R. A note of hybrid GR-SVM for prediction of surface roughness in abrasive water jet machining: A response. *Meccanica* **2017**, *52*, 1993–1994. [CrossRef]

59. Jia, D.; Liang, B.; Yang, Z.; Zhou, Y. Metastable Si-BCN ceramics and their matrix composites developed by inorganic route based on mechanical alloying: Fabrication, microstructures, properties and their relevant basic scientific issues. *Prog. Mater. Sci.* **2018**, *98*, 1–67. [CrossRef]

60. De Jonghe, L.C.; Rahaman, M.N. 4.1 sintering of ceramics. In *Handbook of Advanced Ceramics: Materials, Applications, Processing and Properties*; Academic Press: Cambridge, MA, USA, 2003; pp. 187–264.

61. Wuchina, E.; Opila, E.; Opeka, M.; Fahrenholtz, B.; Talmy, I. UHTCs: Ultra-high temperature ceramic materials for extreme environment applications. *Electrochem. Soc. Interface* **2007**, *16*, 30. [CrossRef]

62. Golla, B.R.; Mukhopadhyay, A.; Basu, B.; Thimmappa, S.K. Review on ultra-high temperature boride ceramics. *Prog. Mater. Sci.* **2020**, *111*, 100651. [CrossRef]

63. Wang, F.; Cheng, L.; Xie, Y.; Jian, J.; Zhang, L. Effects of SiC shape and oxidation on the infrared emissivity properties of ZrB_2–SiC ceramics. *J. Alloys Compd.* **2015**, *625*, 1–7. [CrossRef]

64. Sciti, D.; Savino, R.; Silvestroni, L. Aerothermal behaviour of a SiC fibre-reinforced ZrB_2 sharp component in supersonic regime. *J. Eur. Ceram. Soc.* **2012**, *32*, 1837–1845. [CrossRef]

65. Peng, W.; He, Y.; Wang, X.; Zhu, J.; Han, J. RETRACTED: Thermal protection mechanism of heat pipe in leading edge under hypersonic conditions. *Chin. J. Aeronaut.* **2015**, *28*, 121–132. [CrossRef]

66. Ming, W.; Cao, C.; Xie, Z.; Liu, X.; Xu, Y.; Jiang, Z.; Li, X.; Liu, K.; Guo, X.; Yuan, J. Green manufacturing: A comparative study of renewable dielectrics in the EDM process. *J. Braz. Soc. Mech. Sci. Eng.* **2022**, *44*, 580. [CrossRef]

67. Ming, W.; Zhang, Z.; Wang, S.; Huang, H.; Zhang, Y.; Zhang, Y.; Shen, D. Investigating the energy distribution of workpiece and optimizing process parameters during the EDM of Al6061, Inconel718, and SKD11. *Int. J. Adv. Manuf. Technol.* **2017**, *92*, 4039–4056. [CrossRef]

68. Yang, L.; Ma, W.; Gao, F.; Xi, S. Effect of EDM and Femtosecond-Laser Groove-Texture Collision Frequency on Tribological Properties of 0Cr17Ni7Al Stainless Steel. *Coatings* **2022**, *12*, 611. [CrossRef]

69. Shanbhog, N.; Arunachalam, N.; Bakshi, S.R. Surface integrity studies on ZrB_2 and graphene reinforced ZrB_2 ceramic matrix composite in EDM process. *CIRP J. Manuf. Sci. Technol.* **2022**, *38*, 401–413. [CrossRef]

70. Quarto, M.; Bissacco, G.; D'Urso, G. Machinability and energy efficiency in micro-EDM milling of zirconium boride reinforced with silicon carbide fibers. *Materials* **2019**, *12*, 3920. [CrossRef]

71. Ramulu, M. EDM sinker cutting of a ceramic particulate composite, SiC-TiB sub 2. *Adv. Ceram. Mater. (USA)* **1988**, *3*, 4.

72. Chiang, K.-T. Modeling and analysis of the effects of machining parameters on the performance characteristics in the EDM process of Al_2O_3 + TiC mixed ceramic. *Int. J. Adv. Manuf. Technol.* **2008**, *37*, 523–533. [CrossRef]

73. Patel, K.M.; Pandey, P.M.; Rao, P.V. Determination of an optimum parametric combination using a surface roughness prediction model for EDM of Al_2O_3/SiCw/TiC ceramic composite. *Mater. Manuf. Process.* **2009**, *24*, 675–682. [CrossRef]

74. Puertas, I.; Luis, C.J.; Alvarez, L. Analysis of the influence of EDM parameters on surface quality, MRR and EW of WC–Co. *J. Mater. Process. Technol.* **2004**, *153*, 1026–1032. [CrossRef]

75. Monteverde, F.; Bellosi, A.; Scatteia, L. Processing and properties of ultra-high temperature ceramics for space applications. *Mater. Sci. Eng. A* **2008**, *485*, 415–421. [CrossRef]

76. Li, H.; Wang, Z.; Wang, Y.; Liu, H.; Bai, Y. Micro-EDM drilling of ZrB_2-SiC-graphite composite using micro sheet-cylinder tool electrode. *Int. J. Adv. Manuf. Technol.* **2017**, *92*, 2033–2041. [CrossRef]

77. Malek, O.; Vleugels, J.; Vanmeensel, K.; Van Renterghem, W.; Lauwers, B. Electrical discharge machining of (Nb_xZr_{1-x}) B_2-SiC composites. *Procedia CIRP* **2013**, *6*, 186–191. [CrossRef]

78. Han, W.B.; Zhang, J.H.; Yang, H.Q.; Ding, G.Z. Fabrication and Precision Electromachining Technology of ZrB_2-SiC Ceramic Composites. *Adv. Mater. Res.* **2013**, *753–755*, 267–270. [CrossRef]

79. Zhu, Z.; Guo, D.; Xu, J.; Lin, J.; Lei, J.; Xu, B.; Wu, X.; Wang, X. Processing characteristics of micro electrical discharge machining for surface modification of TiNi shape memory alloys using a TiC powder dielectric. *Micromachines* **2020**, *11*, 1018. [CrossRef]

80. Kumar, S.S.; Varol, T.; Canakci, A.; Kumaran, S.T.; Uthayakumar, M. A review on the performance of the materials by surface modification through EDM. *Int. J. Lightweight Mater. Manuf.* **2021**, *4*, 127–144. [CrossRef]

81. Saha, N.; Chakraborty, S.; Dey, P.P.; Das, P.K. Machining of ZrB2-SiC composites by Wire-EDM technique. *Trans. Indian Ceram. Soc.* **2014**, *73*, 94–97. [CrossRef]

82. Sivasankar, S.; Jeyapaul, R. Characterization of ZrB_2-SiC composites with an analytical study on material removal rate and tool wear rate during electrical discharge machining. *Trans. Can. Soc. Mech. Eng.* **2016**, *40*, 331–349. [CrossRef]

83. Mandal, S.; Chakraborty, S.; Dey, P. A study of mechanical properties and WEDM machinability of spark plasma sintered ZrB2–B4C ceramic composites. *Micron* **2022**, *153*, 103198. [CrossRef]

84. Zhang, Z.; Zhang, Y.; Liu, D.; Zhang, Y.; Zhao, J.; Zhang, G. Bubble Behavior and Its Effect on Surface Integrity in Laser-Induced Plasma Micro-Machining Silicon Wafer. *J. Manuf. Sci. Eng.* **2022**, *144*, 091008. [CrossRef]

85. Zhang, Z.; Qiu, W.; Zhang, G.; Liu, D.; Wang, P. Progress in applications of shockwave induced by short pulsed laser on surface processing. *Opt. Laser Technol.* **2023**, *157*, 108760. [CrossRef]

86. Zhang, Z.; Liu, D.; Zhang, Y.; Xue, T.; Huang, Y.; Zhang, G. Fabrication and droplet impact performance of superhydrophobic Ti6Al4V surface by laser induced plasma micro-machining. *Appl. Surf. Sci.* **2022**, *605*, 154661. [CrossRef]

87. Myronyuk, O.; Baklan, D.; Vasilyev, G.S.; Rodin, A.M.; Vanagas, E. Wetting Patterns of Liquid-Repellent Femtosecond Laser Textured Aluminum Surfaces. *Coatings* **2022**, *12*, 1852. [CrossRef]

88. Bhaskar, V.; Kumar, D.; Singh, K.K. Laser processing of glass fiber reinforced composite material: A review. *Aust. J. Mech. Eng.* **2017**, *17*, 95–108. [CrossRef]

89. Narazaki, A.; Takada, H.; Yoshitomi, D.; Torizuka, K.; Kobayashi, Y. Ultrafast laser processing of ceramics: Comprehensive survey of laser parameters. *J. Laser Appl.* **2021**, *33*, 012009. [CrossRef]

90. Yang, M.; Wang, T.; Wu, M. Ablation behavior of SiC whisker and ZrB_2 particle-filled ZrO_2 sol-gel composite coating under high-intensity continuous laser irradiation. *Ceram. Int.* **2021**, *47*, 26327–26334. [CrossRef]

91. Mahmod, D.S.A.; Glandut, N.; Khan, A.A.; Labbe, J.-C. Surface oxidation of porous ZrB_2-SiC ceramic composites by continuous-wave ytterbium fibre laser. *Appl. Surf. Sci.* **2015**, *357*, 1982–1990. [CrossRef]

92. Wang, A.; Zhao, X.; Huang, M.; Zhang, Z.; Xie, L. A quantitative study of flaw/strength response in ultra-high temperature ceramics based on femtosecond laser method. *Theor. Appl. Fract. Mech.* **2020**, *110*, 102775. [CrossRef]

93. Lonné, Q.; Glandut, N.; Lefort, P. Surface densification of porous ZrB_2–39 mol.% SiC ceramic composites by a laser process. *J. Eur. Ceram. Soc.* **2012**, *32*, 955–963. [CrossRef]

94. Rudolph, P.; Brzezinka, K.-W.; Wäsche, R.; Kautek, W. Physical chemistry of the femtosecond and nanosecond laser–material interaction with SiC and a SiC–TiC–TiB_2 composite ceramic compound. *Appl. Surf. Sci.* **2003**, *208*, 285–291. [CrossRef]

95. Singh, R.P.; Singhal, S. Rotary ultrasonic machining: A review. *Mater. Manuf. Process.* **2016**, *31*, 1795–1824. [CrossRef]

96. Li, H.; Wang, Y.; Wang, Z.; Zhao, Z. Fabrication of ZrB_2–SiC–graphite ceramic micro-nozzle by micro-EDM segmented milling. *J. Micromechanics Microengineering* **2018**, *28*, 105022. [CrossRef]

97. Ramulu, M. Ultrasonic machining effects on the surface finish and strength of silicon carbide ceramics. *Int. J. Manuf. Technol. Manag.* **2005**, *7*, 107–126. [CrossRef]

98. Jia, Y.; Mehta, S.T.; Li, R.; Chowdhury, M.A.R.; Horn, T.; Xu, C. Additive manufacturing of ZrB_2–$ZrSi_2$ ultra-high temperature ceramic composites using an electron beam melting process. *Ceram. Int.* **2021**, *47*, 2397–2405. [CrossRef]

99. Pasagada, V.K.V.; Yang, N.; Xu, C. Electron beam sintering (EBS) process for Ultra-High Temperature Ceramics (UHTCs) and the comparison with traditional UHTC sintering and metal Electron Beam Melting (EBM) processes. *Ceram. Int.* **2022**, *48*, 10174–10186. [CrossRef]

100. Ghasali, E.; Asl, M.S. Microstructural development during spark plasma sintering of ZrB_2–SiC–Ti composite. *Ceram. Int.* **2018**, *44*, 18078–18083. [CrossRef]

101. Adibpur, F.; Tayebifard, S.A.; Zakeri, M.; Asl, M.S. Spark plasma sintering of quadruplet ZrB_2–SiC–ZrC–Cf composites. *Ceram. Int.* **2020**, *46*, 156–164. [CrossRef]

102. Kovaleva, M.; Sirota, V.; Goncharov, I.; Novikov, V.; Yapryntsev, M.; Vagina, O.; Pavlenko, I.; Tyurin, Y. Oxidation Behavior and Microstructural Evolution of ZrB_2–35MoSi$_2$–10Al Composite Coating. *Coatings* **2021**, *11*, 1531. [CrossRef]

103. Kovaleva, M.; Sirota, V.; Goncharov, I.; Novikov, V.; Yapryntsev, M.; Vagina, O.; Pavlenko, I.; Tyurin, Y.; Mogucheva, A. Kinetics Investigation of the Formation of a Gas-Resistant Glass-Forming Layer during the Oxidation of ZrB_2-MoSi$_2$-Y_2O_3-Al Coatings in the Air Atmosphere. *Coatings* **2021**, *11*, 1018. [CrossRef]

104. Vasile, B.S.; Birca, A.C.; Surdu, V.A.; Neacsu, I.A.; Nicoară, A.I. Ceramic composite materials obtained by electron-beam physical vapor deposition used as thermal barriers in the aerospace industry. *Nanomaterials* **2020**, *10*, 370. [CrossRef]

105. Cui, K.; Mao, H.; Zhang, Y.; Wang, J.; Wang, H.; Tan, T.; Fu, T. Microstructure, mechanical properties, and reinforcement mechanism of carbide toughened ZrC-based ultra-high temperature ceramics: A review. *Compos. Interfaces* **2022**, *29*, 729–748. [CrossRef]

106. Mao, H.; Shen, F.; Zhang, Y.; Wang, J.; Cui, K.; Wang, H.; Lv, T.; Fu, T.; Tan, T. Microstructure and mechanical properties of carbide reinforced tic-based ultra-high temperature ceramics: A review. *Coatings* **2021**, *11*, 1444. [CrossRef]

107. Tang, S.; Hu, C. Design, preparation and properties of carbon fiber reinforced ultra-high temperature ceramic composites for aerospace applications: A review. *J. Mater. Sci. Technol.* **2017**, *33*, 117–130. [CrossRef]

108. Han, D.; Mei, H.; Xiao, S.; Dassios, K.G.; Cheng, L. A review on the processing technologies of carbon nanotube/silicon carbide composites. *J. Eur. Ceram. Soc.* **2018**, *38*, 3695–3708. [CrossRef]

109. Nakamura, T.; Oka, T.; Imanari, K.; Shinohara, K.; Ishizaki, M. Development of CMC turbine parts for aero engines. *IHI Eng. Rev.* **2014**, *47*, 29–32.

110. Gautam, S.; Malik, P.; Jain, P. Ceramic composites for aerospace applications. *Diffus. Found.* **2019**, *23*, 31–39.

111. Hart, A.H.; Koizumi, R.; Hamel, J.; Owuor, P.S.; Ito, Y.; Ozden, S.; Bhowmick, S.; Syed Amanulla, S.A.; Tsafack, T.; Keyshar, K. Velcro-inspired SiC fuzzy fibers for aerospace applications. *ACS Appl. Mater. Interfaces* **2017**, *9*, 13742–13750. [CrossRef]

112. Gwon, J.Y.; Jang, S.H.; Kwon, W.T.; Kim, Y.-W. Micro electrical discharge drilling characteristics of conductive SiC–Ti2CN composite. *J. Mech. Sci. Technol.* **2018**, *32*, 3351–3358. [CrossRef]

113. Ming, W.; Xie, Z.; Cao, C.; Liu, M.; Zhang, F.; Yang, Y.; Zhang, S.; Sun, P.; Guo, X. Research on EDM Performance of Renewable Dielectrics under Different Electrodes for Machining SKD11. *Crystals* **2022**, *12*, 291. [CrossRef]

114. Zapata-Solvas, E.; Jayaseelan, D.D.; Lin, H.-T.; Brown, P.; Lee, W.E. Mechanical properties of ZrB2-and HfB2-based ultra-high temperature ceramics fabricated by spark plasma sintering. *J. Eur. Ceram. Soc.* **2013**, *33*, 1373–1386. [CrossRef]

115. Kumar, S.S.; Erdemir, F.; Varol, T.; Kumaran, S.T.; Uthayakumar, M.; Canakci, A. Investigation of WEDM process parameters of Al–SiC–B$_4$C composites using response surface methodology. *Int. J. Lightweight Mater. Manuf.* **2020**, *3*, 127–135. [CrossRef]

116. Marschall, J.; Fletcher, D.G. High-enthalpy test environments, flow modeling and in situ diagnostics for characterizing ultra-high temperature ceramics. *J. Eur. Ceram. Soc.* **2010**, *30*, 2323–2336. [CrossRef]

117. Fattahi, M.; Ershadi, M.N.; Vajdi, M.; Moghanlou, F.S.; Namini, A.S.; Asl, M.S. On the simulation of spark plasma sintered TiB$_2$ ultra high temperature ceramics: A numerical approach. *Ceram. Int.* **2020**, *46*, 14787–14795. [CrossRef]

118. Xia, H.; Zhao, G.; Zhang, Y.; Li, L.; He, N.; Hansen, H.N. Nanosecond laser-induced controllable oxidation of TiB$_2$–TiC ceramic composites for subsequent micro milling. *Ceram. Int.* **2022**, *48*, 2470–2481. [CrossRef]

119. Oliveira, V.; Vilar, R.; Conde, O. Excimer laser ablation of Al$_2$O$_3$–TiC ceramics: Laser induced modifications of surface topography and structure. *Appl. Surf. Sci.* **1998**, *127*, 831–836. [CrossRef]

120. Xing, Y.; Deng, J.; Wu, Z.; Cheng, H. Effect of regular surface textures generated by laser on tribological behavior of Si$_3$N$_4$/TiC ceramic. *Appl. Surf. Sci.* **2013**, *265*, 823–832. [CrossRef]

121. Feng, G.; Li, H.; Yao, X.; Ren, B.; Jia, Y.; Sun, J. Evaluation of ablation resistant ZrC-SiC multilayer coating for SiC coated carbon/carbon composites under oxyacetylene and laser conditions. *Corros. Sci.* **2022**, *205*, 110427. [CrossRef]

122. Jayaseelan, D.D.; Zapata-Solvas, E.; Brown, P.; Lee, W.E. In situ formation of oxidation resistant refractory coatings on SiC-reinforced ZrB$_2$ ultra high temperature ceramics. *J. Am. Ceram. Soc.* **2012**, *95*, 1247–1254. [CrossRef]

123. Best, J.P.; Zechner, J.; Wheeler, J.M.; Schoeppner, R.; Morstein, M.; Michler, J. Small-scale fracture toughness of ceramic thin films: The effects of specimen geometry, ion beam notching and high temperature on chromium nitride toughness evaluation. *Philos. Mag.* **2016**, *96*, 3552–3569. [CrossRef]

124. Uglov, V.V.; Remnev, G.E.; Kuleshov, A.K.; Astashinski, V.M.; Saltymakov, M.S. Formation of hardened layer in WC-TiC-Co alloy by treatment of high intensity pulse ion beam and compression plasma flows. *Surf. Coat. Technol.* **2010**, *204*, 1952–1956. [CrossRef]

125. Wolfe, D.E.; Singh, J.; Narasimhan, K. Synthesis and characterization of multilayered TiC/TiB$_2$ coatings deposited by ion beam assisted, electron beam-physical vapor deposition (EB-PVD). *Surf. Coat. Technol.* **2003**, *165*, 8–25. [CrossRef]

126. Wang, J.; Li, W.-Z.; Shi, B.; Luo, J.-B. Nano-indentation study on the mechanical properties of TiC/Mo multilayers deposited by ion beam assisted deposition. *Surf. Coat. Technol.* **2000**, *128*, 161–165. [CrossRef]

127. Gao, B.; Peng, H.; Liang, Y.; Lin, J.; Chen, B. Electron beam melted TiC/high Nb-TiAl nanocomposite: Microstructure and mechanical property. *Mater. Sci. Eng. A* **2021**, *811*, 141059. [CrossRef]

128. Oh, J.C.; Lee, S. Correlation of microstructure with hardness and fracture properties of (TiC, SiC)/Ti-6Al-4V surface composites fabricated by high-energy electron-beam irradiation. *Surf. Coat. Technol.* **2004**, *179*, 340–348.

129. Kiran, K.; Kumar, K.R.; Chandrasekar, K. Optimization of Abrasive Water Jet Machining Parameters of Al/Tic Using Response Surface Methodology and Modified Artificial Bee Colony Algorithm. In *Nature-Inspired Optimization in Advanced Manufacturing Processes and Systems*; CRC Press: Boca Raton, FL, USA, 2020; pp. 245–258.

130. Ming, W.; Cao, C.; Shen, F.; Zhang, Z.; Liu, K.; Du, J.; Jia, H. Numerical and experimental study on WEDM of BN-AlN-TiB$_2$ composite ceramics based on a fusion FEM model. *J. Manuf. Process.* **2022**, *76*, 138–154. [CrossRef]

131. Ming, W.; Sun, P.; Zhang, Z.; Qiu, W.; Du, J.; Li, X.; Zhang, Y.; Zhang, G.; Liu, K.; Wang, Y. A systematic review of machine learning methods applied to fuel cells in performance evaluation, durability prediction, and application monitoring. *Int. J. Hydrogen Energy* **2022**, *in press*. [CrossRef]

132. Zhang, Y.; Zhang, G.; Zhang, Z.; Zhang, Y.; Huang, Y. Effect of assisted transverse magnetic field on distortion behavior of thin-walled components in WEDM process. *Chin. J. Aeronaut.* **2022**, *35*, 291–307. [CrossRef]

133. Rasaki, S.A.; Zhang, B.; Anbalagam, K.; Thomas, T.; Yang, M. Synthesis and application of nano-structured metal nitrides and carbides: A review. *Prog. Solid State Chem.* **2018**, *50*, 1–15. [CrossRef]

134. Bocanegra-Bernal, M.H.; Matovic, B. Mechanical properties of silicon nitride-based ceramics and its use in structural applications at high temperatures. *Mater. Sci. Eng. A* **2010**, *527*, 1314–1338. [CrossRef]

135. Miyauchi, J.; Kobayashi, Y. Development of silicon nitride turbine rotors. *SAE Trans.* **1985**, *94*, 858–862.

136. Diaz, O.G.; Luna, G.G.; Liao, Z.; Axinte, D. The new challenges of machining Ceramic Matrix Composites (CMCs): Review of surface integrity. *Int. J. Mach. Tools Manuf.* **2019**, *139*, 24–36. [CrossRef]

137. Rashid, A.; Perveen, A.; Jahan, M.P. Understanding novel assisted electrode from a theoretical and experimental perspectives for EDM of aluminum nitride ceramics. *Int. J. Adv. Manuf. Technol.* **2021**, *116*, 2959–2973. [CrossRef]

138. Putyra, P.; Laszkiewicz-Lukasik, J.; Wyżga, P.; Podsiadlo, M.; Smuk, B. The selection of phase composition of silicon nitride ceramics for shaping with the use of EDM machining. *Manuf. Eng.* **2011**, *48*, 35–40.

139. Selvarajan, L.; Narayanan, C.S.; Jeyapaul, R.; Manohar, M. Optimization of EDM process parameters in machining Si$_3$N$_4$-TiN conductive ceramic composites to improve form and orientation tolerances. *Measurement* **2016**, *92*, 114–129. [CrossRef]

140. Schubert, A.; Zeidler, H.; Kühn, R.; Hackert-Oschätzchen, M.; Flemmig, S.; Treffkorn, N. Investigation of ablation behaviour in micro-EDM of nonconductive ceramic composites ATZ and Si$_3$N$_4$-TiN. *Procedia CIRP* **2016**, *42*, 727–732. [CrossRef]

141. Marrocco, V.; Modica, F.; Bellantone, V.; Medri, V.; Fassi, I. Pulse-type influence on the micro-EDM milling machinability of Si$_3$N$_4$-TiN workpieces. *Micromachines* **2020**, *11*, 932. [CrossRef]

142. Bucciotti, F.; Mazzocchi, M.; Bellosi, A. Perspectives of the Si$_3$N$_4$-TiN ceramic composite as a biomaterial and manufacturing of complex-shaped implantable devices by electrical discharge machining (EDM). *J. Appl. Biomater. Biomech.* **2010**, *8*, 28–32.

143. Knowles, M.R.H.; Rutterford, G.; Karnakis, D.; Ferguson, A. Micro-machining of metals, ceramics and polymers using nanosecond lasers. *Int. J. Adv. Manuf. Technol.* **2007**, *33*, 95–102. [CrossRef]

144. Tshabalala, L.C.; Pityana, S. Surface texturing of Si$_3$N$_4$-SiC ceramic tool components by pulsed laser machining. *Surf. Coat. Technol.* **2016**, *289*, 52–60. [CrossRef]

145. Blugan, G.; Herrmann, T.; Graule, T.; Kuebler, J. Laser machining of silicon nitride based composite cantilever structures. *Opt. Lasers Eng.* **2011**, *49*, 1095–1100. [CrossRef]

146. Kandi, K.K.; Thallapalli, N.; Chilakalapalli, S.P.R. Development of silicon nitride-based ceramic radomes—A review. *Int. J. Appl. Ceram. Technol.* **2015**, *12*, 909–920. [CrossRef]

147. Campbell, G.R.; Islam, M.U. Laser machining of silicon nitride base materials. *Mater. Manuf. Process* **1995**, *10*, 509–518. [CrossRef]

148. Vlasova, M.; Alimbekov, M.S.; Zhelezov, P.E.; Mel'Nikov, I.V.; Tokarev, V.N.; Aguilar, P.M.; Kakazey, M.; Reséndiz-González, M.C.; Tapia, R.G. Laser-induced Si$_3$N$_4$-TiN ceramics degradation. *Ceram. Int.* **2020**, *46*, 3668–3674. [CrossRef]

149. Xing, Y.; Luo, C.; Wan, Y.; Huang, P.; Wu, Z.; Zhang, K. Formation of bionic surface textures composed by micro-channels using nanosecond laser on Si$_3$N$_4$-based ceramics. *Ceram. Int.* **2021**, *47*, 12768–12779. [CrossRef]

150. Xing, Y.; Deng, J.; Lian, Y.; Zhang, K.; Zhang, G.; Zhao, J. Multiple nanoscale parallel grooves formed on Si$_3$N$_4$/TiC ceramic by femtosecond pulsed laser. *Appl. Surf. Sci.* **2014**, *289*, 62–71. [CrossRef]

151. Colligon, J.S.; Vishnyakov, V.; Valizadeh, R.; Donnelly, S.E.; Kumashiro, S. Study of nanocrystalline TiN/Si$_3$N$_4$ thin films deposited using a dual ion beam method. *Thin Solid Film.* **2005**, *485*, 148–154. [CrossRef]

152. Mitrofanov, M.I.; Rodin, S.N.; Levitskii, I.V.; Troshkov, S.I.; Sakharov, A.V.; Lundin, W.V.; Evtikhiev, V.P. Ga focused ion beam etching of a Si$_3$N$_4$/GaN substrate for submicron selective epitaxy. *J. Phys. Conf. Ser.* **2017**, *816*, 012009. [CrossRef]

153. Huang, H.; Zhang, Z.; Ming, W.; Xu, Z.; Zhang, Y. A novel numerical predicting method of electric discharge machining process based on specific discharge energy. *Int. J. Adv. Manuf. Technol.* **2017**, *88*, 409–424. [CrossRef]

154. Ming, W.; Hou, J.; Zhang, Z.; Huang, H.; Xu, Z.; Zhang, G.; Huang, Y. Integrated ANN-LWPA for cutting parameter optimization in WEDM. *Int. J. Adv. Manuf. Technol.* **2016**, *84*, 1277–1294. [CrossRef]

155. Ming, W.; Zhang, S.; Zhang, G.; Du, J.; Ma, J.; He, W.; Cao, C.; Liu, K. Progress in modeling of electrical discharge machining process. *Int. J. Heat Mass Transf.* **2022**, *187*, 122563. [CrossRef]

156. Umroh, B.; Ginting, A.; Rahman, M.N.A. CO$_2$ laser machining on alumina ceramic: A review. *IOP Conf. Ser. Mater. Sci. Eng.* **2020**, *1003*, 012131. [CrossRef]